APPLICATION OF 3D PRINTING FOR FRACTURE CONDUCTIVITY TESTING

A Thesis

by

CHINEMEREM EDMOND OBI

Submitted to the Graduate and Professional School of
Texas A&M University
In partial fulfillment of the requirements for the degree of

MASTER OF SCIENCE

Chair of Committee,	Dan Hill,
Co-Chair of Committee,	Ding Zhu
Committee Member	Frederick Chester
Head of Department,	Jeff Spath

August 2021

Major Subject: Petroleum Engineering

ABSTRACT

Using 3D printing technology, fracture conductivity test samples are replicated to overcome the challenge of sample inconsistency. The fracture surface topography is acquired using a laser profilometer, CT scans, and photogrammetry techniques. The developed and printed 3D models are used to make concrete replicates of cement/shale and cement/sand mixtures.

We validate the replicability of these samples based on visualized scans of the fracture surface of the original rock samples, 3D molds, and concrete replicates. The joint roughness coefficient is also used to quantify and validate the replicability of these samples. The replicability ranged from 78% to 99% for the Meremac core using CT scans and DLP printer, and from 75% to 93% for the Austin chalk core using photogrammetry technique and FDM printer. The fracture conductivity results were used as the final check for replicability. The cement/sand mixture replicate C5 and C7 which were cured for relatively similar conditions produced very similar fracture conductivity results.

Based on these results, we stipulate that 3D printing can be applied for fracture conductivity testing to replicate fracture surfaces and experimentally investigate factors that contribute to fracture conductivity. Mechanical properties and surface topography of rock samples dominate fracture conductivity behavior especially at closure stress within the peak strength of the rock sample.

This study is important because the consistency of fracture conductivity samples will provide valuable insights into experimental studies on hydraulic fracturing. The effects of surface topography, proppant distribution, grain size distribution, fluid carrying

ability of fracturing fluids, and several other factors that affect fracture conductivity can now be qualitatively investigated.

DEDICATION

To God

To man

And to the quest for knowledge

ACKNOWLEDGEMENTS

For every iceberg floating there is a greater structure beneath the sea, to every tree standing there is a strong root that you don't see, to every great movie rolling there is the greater crew behind the scenes. To this beauty of a building, you have been a cornerstone.

I sincerely appreciate the CEO and all the efforts he is putting into building the foundations of his life. You shall be a foundation upon which many great pillars are built.

I would like to express my gratitude to Dr. Daniel Hill and Dr. Ding Zhu for their guidance and being part of their research group through my Master's degree. I would also want to thank Dr. Frederick Chester for serving as my committee member and for helping me understand rocks better.

Thanks to Dr. Xiaofeng and Dr. Hiroko in the Handin rock deformation lab for guiding me through rock deformations and every other professor at TAMU whose class I took.

Shout out to Alex for running these FC tests with me, Tohoko my matlab guru, Gabe, and every member of our research group. For your intelligent contributions and all the friends, graduate students who have made this not boring. To you reading this, you deserve some accolades.

Now most importantly my people, *mpa*, *mma*, *pempeles* and *ariboy* for the love and support, you are my home and *I am coming home*.

To the one omniscience God, Thank you.

CONTRIBUTORS AND FUNDING SOURCES

Contributors

This work was supervised by a thesis committee consisting of Dr. Dan Hill, Dr. Ding Zhu, of the Harold Vance Department of Petroleum Engineering, and Dr. Frederick Chester of the Department of geophysics at Texas A&M University.

The source code for visualizing the profilometer data is from the Fracture conductivity group and was modified by Tohoko Tajima. Alex Fojtasek ran the Fracture conductivity tests with me. Gabe Tateman helped with the 3D printers. Technical assistance from John Maldonado.

TABLE OF CONTENTS

Page

LIST OF FIGURES

Page

LIST OF TABLES

Page

1. INTRODUCTION

1.1 Background

The current advancements in the oil and gas industry are at a point where hydraulic fracturing is mostly required for optimal exploitation of these unconventional reserves which are fine-grained, heterogeneous with complex mineralogy. To forecast the profitability of producing these shales, accurate knowledge of the fracture conductivity that is, the product of the fracture width and fracture permeability, is required. The fracture conductivity of a rock sample can be investigated experimentally using the Modified API Fracture Conductivity Test. 3D printing has gained traction in recent years as a very applicable technology to many fields such as biological medicine, education, aviation, engineering, and most recently rock mechanics. The true investigation of the mechanical and related behavior of rock samples by conventional methods over the years has been limited by the replicability of these tests which is mainly due to significant heterogeneity (Jiang, et al., 2015).

Experimental fracture conductivity tests are highly dependent on the effective closure stress, and the sample surface topography, that is fracture roughness and waviness. The fracture conductivity is a function of the rock strength and proppant strength while the rock surface topography is significantly affected by created asperities due to planes of weakness and heterogeneity (Guerra, 2019), (Suarez-Rivera, et al., 2013) (Enriquez, et al., 2016).

With the use of 3D printing to replicate any free form and property uniformness, consistency can be achieved and thus mitigating this challenge of inconsistency in sample properties used for fracture conductivity testing.

1.2 Literature Review

With the surge in hydraulic fracturing operations to optimally exploit unconventional reserves, a lot of work has been done on fracture conductivity testing for efficient well stimulation. Likewise, with the rapid growth in additive manufacturing and 3D printing technologies, sufficient research and application of these technologies for prototyping, tooling, biomedical, automotive and aerospace are available. Although the application and literature on additive manufacturing and 3D printing is limited in the oil and gas industry especially for rock mechanics, and well stimulation. This section elaborates the work done so far, in hydraulic fracturing, experimental fracture conductivity testing, and application of additive manufacturing and 3D printing to rock mechanics and rock engineering.

1.2.1 Hydraulic Fracturing in the Field

The optimal exploitation of unconventional resources, which are tight and have relatively no economically feasible permeability will require high conductive flow paths to be created by hydraulic fracturing especially in shales. This technique of inducing pathways in the formation by the mechanical impact of fluids which are most commonly water with varying additives above the formation breakdown pressure, hydraulic fracturing, was first introduced experimentally in 1947 in Hugoton gas field, Grant county of Kansas by Stanolind Oil. (Montgomery & Smith, 2010).

To maintain the integrity of the fracture network, that is keep it propped open even after pumping operations have stopped, proppants are also pumped with the fracturing fluid. There are several sizes of proppant and their selection is dependent on formation closure stress, proppant strength, and proppant transport characterization. Optimal hydraulic fracturing design is dependent on the selection of proppant, fracturing fluid type, and its additives (Elsarawy & Nasr-El-Din, 2018) (Gupta, Rai, & Sondergeld, 2019).

1.2.2 Experimental Investigation of Fracture Conductivity

The extensive study of fracture conductivity has been carried out experimentally, from Cooke's work in the 1970s to date. (Cooke Jr, 1973) studied environmental effects such as type of fluid present and temperature, and flowrate on the conductivity. Several studies such as fracture conductivity behavior in specific formations, gel residue, proppant grain size distribution on hydraulic fracture conductivity have been investigated by several students of the fracture conductivity group at Teas A&M University with appreciable results including minute details as to how proppant size variation affect conductivity, (Guerra, 2019) (Zhang, 2014), (Copeland, 2020), (Marpaung, 2007).

For these laboratory investigations, effects such as proppant size, proppant crushing, fines migration in the formation, the mineralogy of rock, fluid chemistry, volcanic ash, and presence of complex ions which could induce diagenesis have all been carried out also (Gupta, Rai, & Sondergeld, 2019) (Mittal, Rai, & Sondergeld, Proppant-Conductivity Testing Under Simulated Reservoir Conditions: Impact of Crushing, Embedment, and Diagenesis on Long-Term Production in Shales, 2018) (Mittal, Rai, & Sondergeld, 2017). Comparing field and lab results (Barree & Duenckel, 2019) concluded

that the effective permeability of the proppant pack is less than 5% of the permeability measured in the lab. With all this work done so far in experimental fracture conductivity testing, one constant challenge of these studies is the replicability of results on a particular rock sample with the same defined surface topography. Fracture conductivity is quantified mathematically as in **Eq. 1.1.**

$$C_f = k_f w_f \tag{1.1}$$

1.2.3 Additive Manufacturing and 3D Printing applications for Fracture Conductivity Testing

A viable solution to the challenge of test replicability with a rock sample of the same defined surface topography is the application of Additive Manufacturing and/or 3D printing to creating samples used for fracture conductivity testing in the lab. Since the integrity of the fracture face of these samples is lost, most times after a single test of applying several uniaxial stresses which could range up to several thousand psi.

Additive manufacturing and 3D printing have been applied over the years to other engineering fields such as Biomedical, Aerospace, Automotive, and the Military, for rapid prototyping, tooling, and the creation of parts that are difficult to machine (Camisa, Verma, Marler, & Madlinger, 2014). In the oil and gas industry, these fabrication technologies which have also been applied for prototyping purposes are now used to make or replicate functional parts to support processes. Several studies on the applications of Additive manufacturing and 3D printing to rock mechanics and rock engineering have also been reported with appreciable success (Isleyen & Duzgun, 2018) (Osniga, Zambrano-Narvez, & Chalaturnyk, 2015). Based on Additive manufacturing and 3D

printing growing applicability and their need in studies that require consistency in replicability such as experimental fracture conductivity measurements, this study will further apply these technologies for fracture conductivity testing. It is however vital to make a clear distinction between both Additive manufacturing and 3D printing. Additive manufacturing involves creating volumes of material by combining several layers of material, also keeping in mind the functional purpose of the technology while 3D printing entails producing a part directly from a CAD file. Figure 1 shows a clear distinction of both Additive manufacturing and 3D printing. (Shawn & Jennings, 2014). Similarly, these technologies benefit the industry by reducing the lead time to fabricate a material, better efficiency in replicating complex designs, and achieving enhanced functionality (Burns & Wangenheim, 2019)

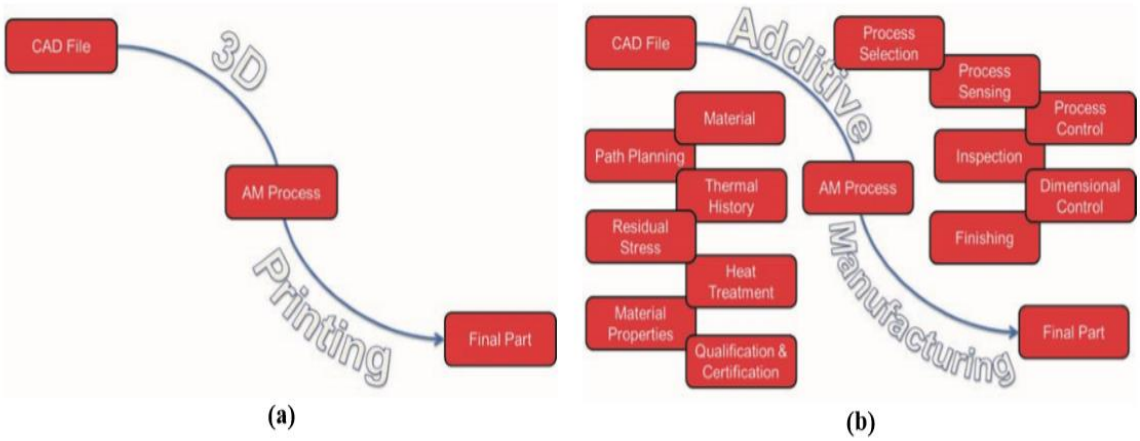

Figure 1-1: Depiction of 3D printing versus Additive Manufacturing Reprinted from (Shawn & Jennings, 2014)

3D Printing is a fast prototyping technique that reduces material preparation time, allows one to achieve precision and flexibility in the control sample geometry specifically

to produce predefined fractures or roughness with a high degree of homogeneity (Jiang, Zhao, Gao, & Zhao, 2016). Although only a few studies have been carried out concerning the use of 3DP materials such as resin or plastic material (PLA) in rock mechanics, Table 1 shows a compilation of base materials and their additive technologies categorized by their respective processes.

Table 1: Additive Manufacturing Primary Technologies Reprinted from (Camisa et al, 2014)

Category	Additive Technologies	Base Materials
Extrusion	Fused deposition modeling (FDM)	Thermoplastics, eutectic metals
Granular	Selective laser sintering (SLS)	Thermoplastics, metal & ceramic powders
	Direct metal laser sintering (DMLS)	Almost any metal alloy
	Electron beam melting (EBM)	Titanium Alloys
	Powder bed and inkjet 3D printing	Paper, plastic film
	Plaster-based 3D printing (PP)	Plaster, colored plaster
Laminated	Laminated object manufacturing (LOM)	Paper, metal foil, plastic film
Light Polymerized	Sterolithography (SLA)	Photopolymer
	Digital Light Processing (DLP)	Photopolymer

1.3 Problem Description, Objectives, and significance

The true investigation of the mechanical and related behavior of rock samples by conventional methods over the years has been limited by the replicability of these tests which is mainly due to significant heterogeneity (Jiang, et al., 2015).

To apply 3D printing technology to fracture conductivity testing, this study would implement the following objectives:

(1) review of current applications of 3D printing to rock mechanics and well stimulation

(2) Replicate fracture conductivity samples with analog mechanical properties and surface topography.

(3) investigation of the benefits of sample consistency to fracture conductivity testing.

(4) Parametric study using the replicate samples to modify fracture conductivity correlations based on rock surface consistency.

(5) propose a workflow to consistently replicate fracture conductivity test samples.

With the use of 3D printing to replicate any free form and property uniformness, consistency can be achieved and thus mitigating this challenge of inconsistency in sample properties used for fracture conductivity testing. Achieving fracture conductivity test sample replicability with defined rock strength and surface topography will allow true investigation by conducting parametric studies. A particular parameter such as proppant distribution, proppant size, proppant type can be controlled while keeping every other parameter/condition fixed. These would help understand how each parameter truly affects the fracture conductivity. Based on this, correlations between these parameters and fracture conductivity and be developed or modified.

The proposed workflow to replicate samples by using 3D printing also gives an advantage of being able to create mated samples. In some cases, fracture conductivity

samples are not fractured evenly and thus bottom and top halves do not match perfectly. This creates an artificial conductivity and in worst case an infinite conductivity where the sample cannot be tested.

1.4 Experimental Approach

The proposed workflow will involve creating a mold with 3D printing technology suitable for fracture conductivity test. The surface topography of a fractured core sample is first scanned with a profilometer/CT Scan/photogrammetry technique. This is converted to a 3D fracture surface profile using CAD and/or the MATLAB code as developed by (Nieto, 2007). This model is used as input to print out a 3D mold and subsequently, the mold is used to make sample replicates (Isleyen & Duzgun, 2018). These replicates based on how they are made are mated. Fracture conductivity is then determined with both original and replicate samples. The steps are briefly listed as follows:

1. Collect Fracture surface data
2. 3D model/ printing 3D mold
3. Casting concrete to replicate sample
4. Characterization/ Replicability check of Fracture surface and properties
5. Perform experimental fracture conductivity tests with original and replicate
6. Scan Fracture surfaces again for both original and replicate
7. Result analysis and validation

1.5 Thesis Outline

Chapter 1 presents the background of this study and literature review on the 3D printing technology so far and its application to rock engineering and rock mechanics, and

the progress made so far with experimental Fracture conductivity testing (Guerra, 2019) (Copeland, 2020).

Chapter 2 discusses the Methodology of this work, from acquiring fracture surface topography using the profilometer, and processing the data, to steps in creating sample replicates with the printed 3D mold and then testing the fracture conductivity of the replicates. It also discusses the methods of investigating the mechanical properties, mineralogy, and heterogeneity of created samples (Osniga et al, 2015).

Chapter 3 presents the results of the replication process . A comparative analysis of the surface topography of the original rock sample, 3D mold and replicate by the method of joint roughness coefficient as proposed by several works of literature (Tse & Cruden, 1979), (Odling, 1994) (Kulatilake, et al., 2006) (Zhang, et al., 2014). The results of fracture conductivity tests on both original rock samples and replicate are also presented as a measure of the success of replicability. These results can be used to develop standard correlations between parameters that affect fracture conductivity (Awokele, 2013).
Chapter 4 presents the conclusions of this work, limitations, and some recommendations for future work.

2. EXPERIMENTAL DESIGN AND METHODOLOGY

2.1 Introduction

In this chapter, we explain the Methodology of this work, from acquiring fracture surface topography using the profilometer, Computed Tomography (CT) scan, photogrammetry techniques, and processing the data, to steps in creating sample replicates with the printed 3D mold and then testing the fracture conductivity of the replicates. It also discusses the methods of investigating the mechanical properties, mineralogy, and heterogeneity of created samples (Osniga et al, 2015).

As suggested by (Stimpson, 1968), modeling materials for engineering rock mechanics applications, granular materials can be cemented with plaster, cement, oil/wax, resin/plastics or clay. For this study fracture conductivity test samples will be modeled with plaster and cement in their appropriate proportions and a comparative analysis of both cementation materials carried out based on resulting mechanical properties and replicability and fracture conductivity.

To optimally replicate the strength, surface topography, and heterogeneity of a sample, the original rock type is crushed into the granular size of <1mm and <3mm as suggested by (Isleyen & Duzgun, 2018) since particle size greatly affect topography replicability. Also, material strength is greatly dependent on porosity and cementation thus using the same granular material as the original rock sample for modeling will increase chances of consistency in porosity hence mechanical properties (Li & Aubertin, 2003) (Al-Tahini, et al., 2006)

Unpropped fracture conductivity calculation has been well studied in acid fracturing where fracture conductivity is created by unevenly etched fracture faces. Conductivity correlations for unpropped rough fractures were derived by Nierode and Kruk (1973), Gong et al. (1999), Mou et al. (2011, and Deng et al. (2012).

2.2 Sample Replication

Bearing in mind that the main aim of this study is to replicate a fracture conductivity sample both in fracture surface roughness and mechanical behavior as close as possible, the following sub-sections discuss the work done to achieve this.

2.2.1 Acquisition of Fracture Surface Profile

To accurately capture the fracture face for the 3D model, the profilometer, CT scan, and photogrammetry techniques were used. Based on the accuracy of replicability and ease of producibility photogrammetry was chosen as the best technique moving forward.

(Isleyen & Duzgun, 2018) also used photogrammetry for their study. To capture the surface, a digital SLR camera (Sonny alpha a6400 for this case) is used to take photos from different angles of the sample to be reproduced. We then used the Meshroom software for processing these images to a 3D model (AliceVision, 2021).

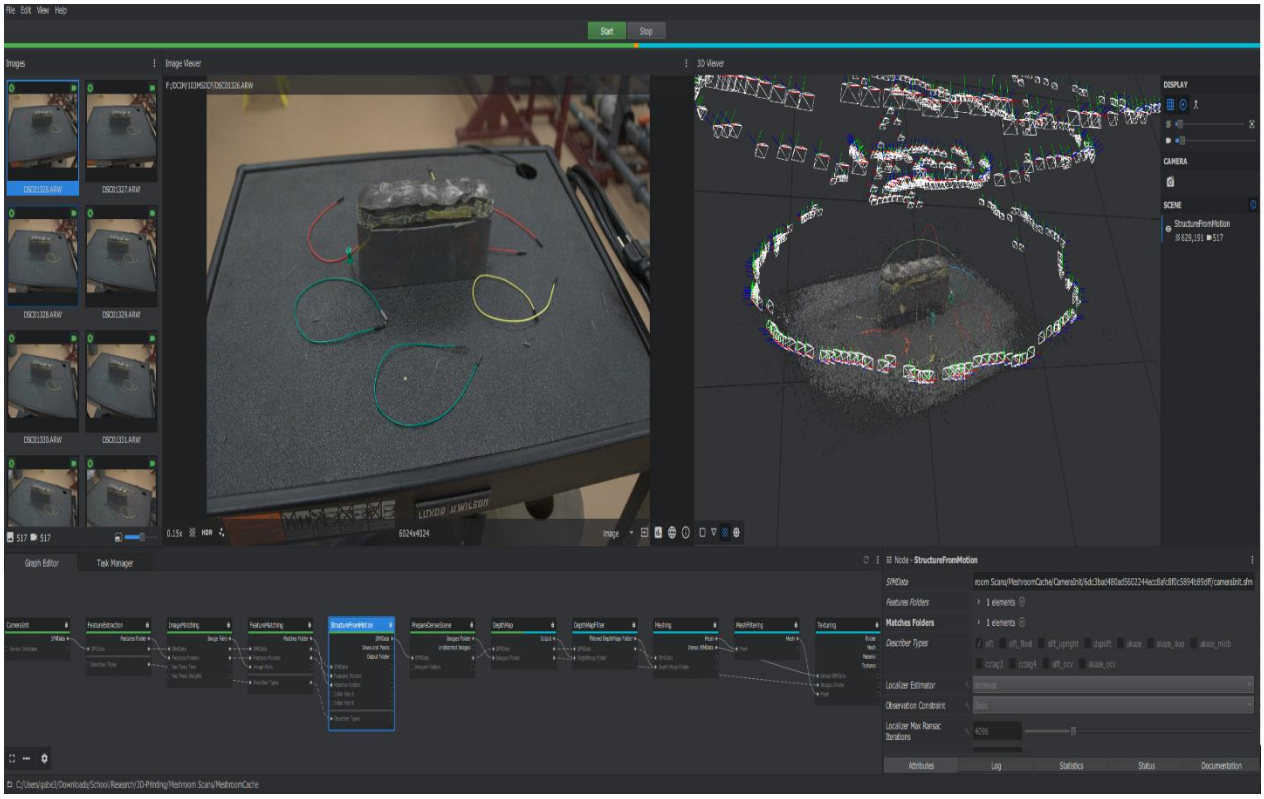

Figure 2-1: Rendering of 3D model by photogrammetry (Meshroom software)

2.2.2 3D Model/3D Model Printing

The 3D model is obtained in stereolithographic format then printed out in solid forms with the 3D printer. The raw material for the mold is environmentally friendly and relatively cheap Polylactic acid. A typical 3D printer is Fused Deposition Modelling which uses an extrusion mechanism to deposit a thermoplastic such as PLA in a predefined Computer Numerical Control tool path. Another common 3D printer is the Digital Light Processing which uses an ultraviolet screen and liquid photo-curing to create objects. Common challenges when using the Fused Deposition Modelling printer are related to the diameter of the nozzle, the cooling of the extruded thermoplastic, and filament feed. Challenges of using the Digital Light Processing are related to UV screen resolution, and

post-processing of 3D printed objects. Although, Fused Deposition Modelling printed objects are relatively strong since thermoplastic is the raw material used. The print time is relatively much with increasing time as required resolution increases. The Digital Light Processing print time does not significantly increase with the required resolution but the 3D printed object would have to be exposed to ultraviolet light for final curing. This can increase the production time by some hours. To overcome these challenges, we use both printer types for various purposes as the case may be. We commonly use the Fused Deposition Modelling to make molds for concrete casting (replica build) and use the Digital Light Processing to print the 3D models of the fracture face. The figures below show the printer types and typical use for this study.

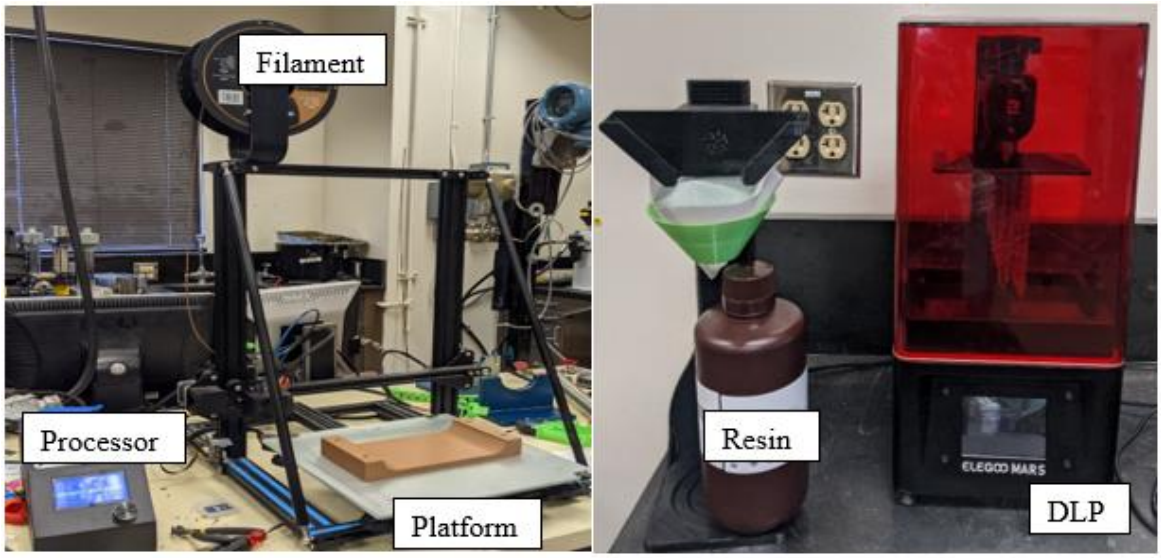

Figure 2-2: 3D printers used for the study, Fused Deposition Modelling (left), Digital Light Processing (right)

2.2.3 Concrete Casting

After printing out the 3D mold, the following steps are then used to make a replicate of the 3D model.

1) Clean 3D printed fracture conductivity model and mold, then apply grease on surfaces carefully to make a thin coat over every surface that might come in contact with concrete mixture. This is to prevent leaks and allow ease of taking replicate apart after without damage.
2) Secure 3D mold together with 3D model inside.
3) Mix cement with sand or shale (depending on replicate type to be made.), water in 1:1:0.5. Stir thoroughly till the consistency is achieved. Use clean and dry shale cuttings for shale-based concretes. Use Particle size <1mm and <3mm for better roughness and strength replicability respectively as suggested by (Isleyen & Duzgun, 2018).
4) For fracture conductivity samples made entirely of cement, 500g of cement should be sufficient.
5) Carefully pour concrete into 3D mold with 3D model inside. Smooth the concrete top (sample bottom) to reduce post-curing smoothing. Allow sample to cure overnight (depend on cement type used).
6) Use the grinder to smooth the sample bottom after it has cured
7) Use acetone to brush off grease from body of sample to ease sample prep for fracture conductivity.
8) Coat samples with concrete sealant. This prevents the sample damage by epoxy infiltration during sample prep.

9) Note the direction of flow as established on the original fracture conductivity sample. Use laser profilometer to scan replicate for comparative analysis. This is described in the subsequent chapter.

2.2.4 Replica Validation

Through the process of fracture conductivity sample replication, there is some change in the degree of roughness. To validate the reproducibility of the fracture face, the laser profilometer is used to capture fracture face data. This moves the sample in both length and width of the sample while the laser measures the roughness amplitude in the height direction. The output from the laser profilometer at the end of the scan is a text file with measured x, y, and z data points of the fracture face. The MATLAB program developed by (Nieto, 2007) is then used to generate a 3D fracture surface profile. Visual analysis of these plots is used as the first guide to replicability check.

This visual comparison highly depends on the viewer, we, therefore, use statistical models from literature such as ((Kulatilake et al. 2006) (Odling, 1994) (Zhang, et al. 2014) (Tse & Cruden, 1979) (Yu & Vayssade, 1991) (Tatone & Grasselli, 2010) (Jang, Kang, & Jang, 2014) to quantify roughness level. The root-mean-square of the surface profile's first derivative noted as the Z_2 parameter and the roughness profile index (R_p) are the roughness level used in this work. These are expressed as Eq. 2.1. and Eq. 2.2 respectively (Woodman, Murphy, & Thomas, 2017).

$$Z_2 = \left[\frac{1}{L}\sum_{i=1}^{n-1}\frac{(y_{i+1}-y_i)^2}{x_{i+1}-x_i}\right]^{\frac{1}{2}} \quad 2.1$$

$$R_p = \frac{\left[\sum_{i=1}^{n-1}(x_{i+1}-x_i)^2+(y_{i+1}-y_i)^2\right]^{\frac{1}{2}}}{L} \quad 2.2$$

(Barton & Choubey, 1977) proposed the visual ten standard joint roughness profiles shown in Fig 2.1. Following this, several relationships between Z_2 and joint roughness coefficient have been developed by (Tse & Cruden, 1979) (Yu & Vayssade, 1991) (Tatone & Grasselli, 2010) (Jang, Kang, & Jang, 2014) as Eqs. 2.3-2.6 respectively.

$$JRC = 32.3 + 32.47 \log(Z_2) \quad 2.3$$

$$JRC = 61.79Z_2 - 3.47 \quad 2.4$$

$$JRC = 51.85(Z_2)^{0.60} - 10.37 \quad 2.5$$

$$JRC = 51.16(Z_2)^{0.531} - 11.44 \quad 2.6$$

Likewise, relationships between R_p and JRC have also been proposed by (Maerz, et al. 1990, Yu & Vayssade, 1991 ,Jang, et al. 2014) as Eqs. 2.7-2.9 respectively.

$$JRC = 411.1(R_p - 1) \quad 2.7$$

$$JRC = 92.07 \sqrt{R_p - 1} - 3.28 \quad 2.8$$

$$JRC = 65.9 \left(R_p - 1\right)^{0.302} - 9.65 \quad 2.9$$

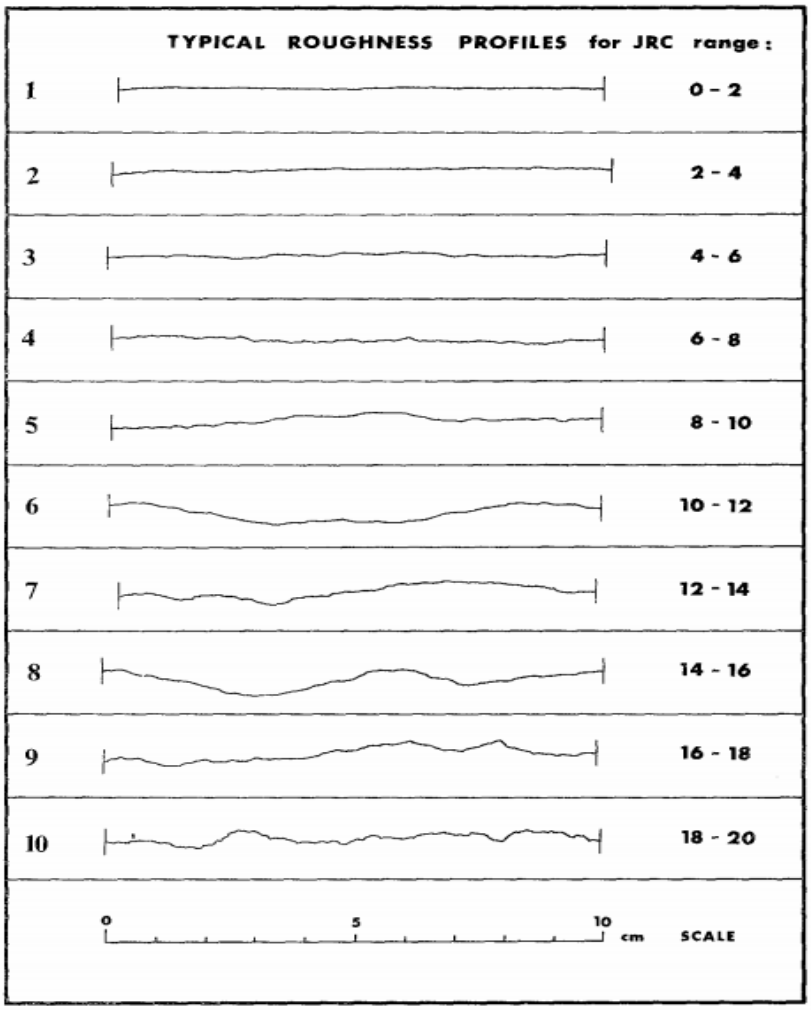

Figure 2-3:Roughness profiles and the typical range of JRC values associated with each one (Barton & Choubey, 1977)

2.3 Experimental Fracture conductivity Testing (Propped)

Fracture conductivity testing in the laboratory involves flowing fluid, typically nitrogen gas, through opposite fractured rock surfaces. The fractured rock is propped with the desired proppant type. Uniaxial confining stress is applied to the sample while the flow rate and differential pressure of the gas flow is measured. Here we explain the

experimental setup, procedures, and underlying principles of this experiment. Similar steps for sample preparation were used as described by (Copeland, 2020).

2.3.1 Experiment Design and Equipment

The fracture conductivity testing setup can be modified to meet specific testing conditions. This study is conducted under standard conditions so no specific modifications were made (API-RP-61, 1989). The basic components we used to set up our fracture conductivity test are; GCTS hydraulic load frame, GCTS system control & data acquisition software, Modified API fracture conductivity cell, pressurized nitrogen cylinder (nitrogen supply), gas flowmeter, cell and differential pressure transducers, backpressure regulator.

Detailed explanations of each of these components have been reported over the years by the fracture conductivity research group at Texas A&M University ((Marpaung, 2007), (Awokele, 2013), (Zhang, 2014), (Winner, 2018) (Guerra, 2019), (Copeland, 2020)).

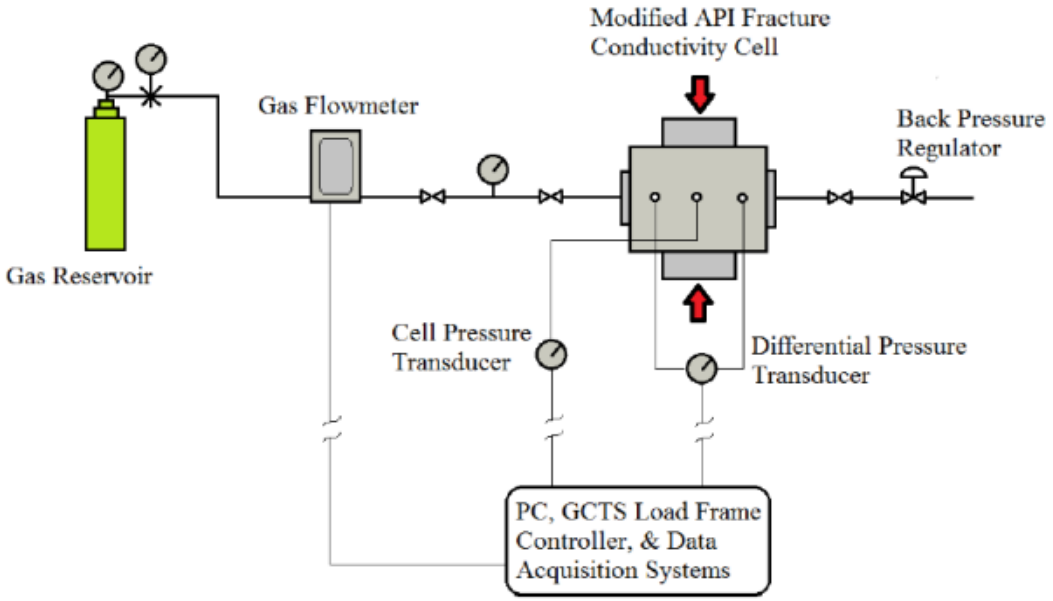

Figure 2-4: Schematic of experimental set up (image from Guerra, 2019)

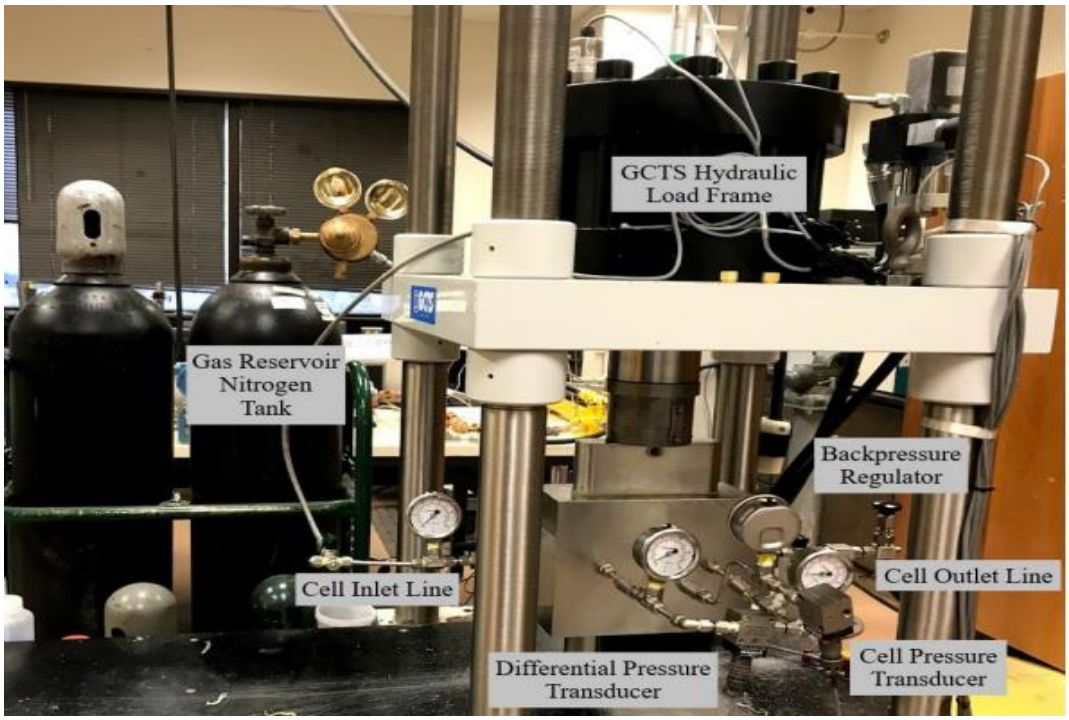

Figure 2-5: experimental set up as seen in our lab **(image from Copeland, 2020)**

2.3.2 Experiment Principle/Underlying Equation

Laboratory fracture conductivity testing is based on two flow equations Darcy (**Eq. 2.10**) and Forchheimer (**Eq. 2.11**) depending on the flow regime.

$$-\frac{dp}{dl} = \frac{\mu v}{k_f} \quad 2.10$$

$$-\frac{dp}{dl} = \frac{\mu v}{k_f} + \beta \rho_f v^2 \quad 2.11$$

$-\frac{dp}{dl}$ is the pressure drop per unit length, μ is fluid viscosity (cP), v is the fluid velocity, k_f is the fracture permeability (md), ρ_f is the fluid density (kg/m^3), and β is the inertial factor for turbulent flow. The additional quadratic correction term in **Eq. 2.11** makes it effective over the range of velocities (Tek, Coats, & Katz, 1962).

Based on their study, Awokele (2013), Zhang (2014) suggest the use of the Forchheimer equation for nitrogen flow rates through the fracture higher than 0.9 L/min and 0.8 L/min respectively. Nonetheless, the Darcy equation can still be applied for flowrates below 2 L/min, where there is a linear relationship between flowrate and pressure gradient (Winner, 2018). Following **Eq. 2.10** for a Darcy flow regime inside the fracture, **Eq. 2.12** is derived (Tek, Coats, & Katz, 1962), (Copeland, 2020).

$$\frac{M p_{cell}\, \Delta P}{ZRTL} = \frac{\mu \rho}{h_f} \frac{1}{(k_f w_f)} \quad 2.12$$

Where M is the molecular weight kg/mol),

p_{cell} is the cell pressure (P_a),

Δp is the differential pressure (P_a),

Z is the gas compressibility factor,

R is the universal gas constant $J/\,mol.K$,

T is the temperature (K),

L is the length of fracture over the entire range of pressure drop (m),

μ is the viscosity of gas $(P_a.s)$,

ρ_f is the fluid density (kg/m^3),

q is the volumetric flow rate of gas (m^3/s),

h_f is the height of the fracture (sample width) (m),

k_f is the fracture permeability(m^2),

w_f is the fracture width (m^2).

Eq. 2.3 can be compared to the equation of a straight line $Y = mx + c$ and graphed as shown below. The inverse of the slope of best fit is related to the fracture conductivity.

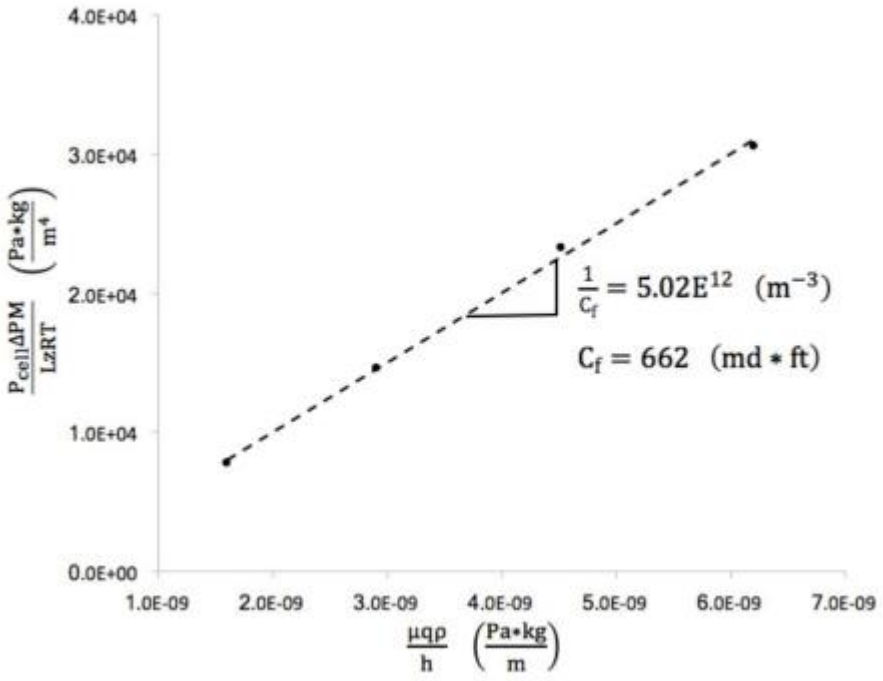

Figure 2-6: Graphical representation for estimating Fracture Conductivity in Darcy flow.

When flow inside the fracture is beyond the Darcy regime (approximately greater than 2 L/min), **Eq. 2.13** bases on the Forchheimer equation is used.

$$\frac{Mp_{cell}\,\Delta P}{zRTL\mu\rho q} = \frac{\beta}{w_f^2}\frac{\rho q}{h_f\mu} + \frac{1}{(k_f w_f)} \qquad 2.13$$

The variables in **Eq. 2.13** are similar as defined by **Eq. 2.12.** The β $(1/m^2)$ is the inertial factor. Likewise, **Eq. 2.13** can be graphed as shown below and compared to the equation of a straight line. For this case, the inverse of the y-intercept of the line of best fit is the fracture conductivity.

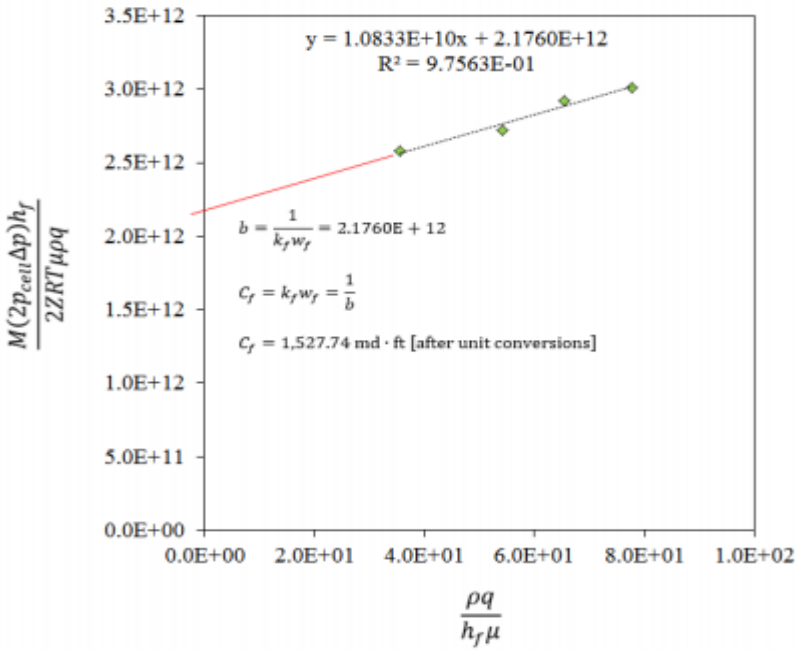

Figure 2-7: Graphical representation of the fracture conductivity for non-Darcy flow (from Guerra, 2019)

2.3.3 Experimental Procedures

To estimate the fracture conductivity of the samples in the laboratory, follow the procedures as stated below. The sample should be handled with extreme caution and

always kept vertical after placing proppants. This is to maintain the integrity of proppant placement and the accuracy in estimation of propped fracture conductivity. Ensure to calibrate the differential and cell pressure transducers before testing any sample (API-RP-61, 1989). After epoxying and prepping the sample for fracture conductivity test with the procedures described by Copeland, (2020), follow these procedures to run test.

1. Log into the laboratory computer and turn on the GCTS control box.
2. Turn on the flowmeter, ensure the regulator valve attached to the nitrogen tank is closed then open the main valve to pressurize the tank.
3. Make five small window cuts through epoxy to expose fracture to the atmosphere. These cuts should align with the flow inlet and outlet, differential, and cell pressure ports on the Modified API cell. See the figure below for reference and cut measurements of each window.
4. Tightly wrap a layer of sealant tape around the sample in six locations (grease areas to be wrapped first). This mitigates pressure leak-off and nitrogen channeling around the sample. See the figure below for reference and wrapping style.
5. Wrap three layers of sealant tape firmly around both rubber O-rings located at the tops of the pistons.
6. Place screens in both endcaps. This prevents proppant migration into the flowlines.
7. Apply a thin coating of clear high-pressure vacuum grease onto the epoxy surface. Avoid greasing below the window cuts. The aim is to prevent grease

in or close to the fracture after it is inserted into the Modified API cell. Also, apply a thin coat to the tape wrapped around the pistons.

8. On the black metal surface to the left of the GCTS load frame, Place the bottom piston inside the black bracket with the port hole facing forward. The port hole should align with the bracket gap.
9. Noting the top of the Modified API cell, A and B are engraved on the sides of the cell and oriented in the up-right direction. Align the bottom of the cell cavity with the top of the piston. The three pressure ports on the front should face forward. Firmly press the cell until it rests evenly on the bottom bracket.
10. Align the front of the sample above the cell cavity and push the sample down carefully into the cavity (use the hydraulic press if needed).
11. Place the top piston with the taped side on top of the sample in the cell
12. Center the top piston under the load press by gently moving the bottom piston and bracket. The top piston will jam in the cavity if not in both x and y directions.
13. Insert and tighten the respective plugs into the top and bottom piston ports.
14. Open the GCTS CATS software.
15. In the "System" drop-down window, select "Configuration" and select "GCTS_1646".
16. In the "Views" drop-down window, select "Load Screen Layout" and select the desired screen layout. The base caseload screen layout should have digital

views for cell pressure, differential pressure, axial displacement, and axial load (see figure below).

17. Turn on the pump by selecting the pump icon and clicking "On".
18. In the "System" drop-down menu, select "Configuration" and "Synchronize".
19. Load the sample to a desired first closure stress (100 psi) by following these steps:
    a. Click the Projects icon.
    b. Select the project.
    c. Click the right arrow.
    d. Enter the sample information.
    e. Click ok.
    f. Click the right arrow.
    g. Click “New” and enter the “100 psi” for the ID.
    h. Click the right arrow.
    i. Select “100 psi”.
    j. Click “Execute”
20. Click “Run”. The system will begin lowering the load press.
21. Monitor the press and top piston, then insert the screens into the pressure ports on the front of the cell to prevent proppant migration into the transducer lines.
22. When the sample is loaded to closure stress of 100 psi or 4.8 kN, Insert and tightly screw the endcaps onto the correct sides of the cell. The endcap

engraved with an “A” should be inserted into the side of the cell also engraved with an “A”.

23. Tightly attach the differential and cell pressure lines to the front of the cell.
24. The differential and cell pressure digital readings should be close to zero. To zero readings, select “Tools” and select “Inputs Offsets”.
25. Attach the inlet and outlet flow lines to the respective endcaps tightly.
26. Close the backpressure valve tightly.
27. Slowly pressurize the cell to a cell pressure of 30 psi with nitrogen flowrate less than 0.1 L/min. This prevents proppant channeling.
28. Slowly open the backpressure valve to allow flow into the cell until a desired flowrate or differential pressure is reached.
    a. Keep the flow below 2 L/min to prevent proppant channeling.
    b. Keep the differential pressure below 3 psi so as not to damage the transducer membrane.
    c. Use the same starting flow rate for each load stage.
29. Record the axial displacement, flowrate, cell pressure, and differential pressure.
30. At each closure stress, take 4 measurements. Establish target pressure drops for average fracture conductivity measurements. Divide the first differential pressure by 4, the value will be the change in pressure between measurements.
31. Close the backpressure regulator slowly to reach the next target differential pressure and record required data.

32. Repeat Steps 32 and 33 until 4 readings are recorded.
33. Twist the nitrogen regulator valve to the left and close the system off to nitrogen flow from the tank.
34. In the GCTS software, click “Stop”.
35. Enter the new closure stress “200 psi” for the new specimen ID.
36. Select "200psi", click "Execute" and click "Run". The system will now load the sample to closure stress of 200 psi.
37. When the cell pressure reaches ~10 psi while watching the differential pressures and flowrates.
38. Once the sample is loaded to closure stress of 200 psi and the cell pressure is ~0 psi, close the backpressure valve. Repeat Steps 26 through 32.
39. Repeat Steps 32 through 34, but for closure stress of 300 psi. These steps should be followed until four measurements are taken at closure stresses 100 psi, 200 psi, 300 psi, and 400 psi. Using the flowrates, differential pressures, axial displacements, and cell pressures recorded, an average fracture conductivity valve can be calculated at each closure stress.
40. After the final reading is recorded at closure stress of 400 psi, close the main valve on the nitrogen tank. Open the backpressure valve to bleed off the pressure. Be cautious of the differential pressures while doing this.
41. In the GCTS software, load the sample to 100 psi again.
42. When the nitrogen tank gauge reads 0 psi, twist the nitrogen regulator valve to the left and close off the system to the nitrogen tank.

43. Completely open the backpressure valve as the cell pressure reaches ~10 psi.
44. At ~0 psi cell pressure and differential pressure, remove the inlet and outlet lines, pressure transducer lines, and endcaps.
45. Click “Stop” on the GCTS software.
46. Enter “unload” for the new specimen ID, and select the unload option.
47. Once the axial displacement is ~0 mm, shut the pump off.
48. Click “File” and select “Shut Down Controller”.
49. Turn off the controller.
50. Remove and separate the cell and pistons. Use the hydraulic press to gently push out the bottom piston and sample.

2.4 Challenges and Considerations

The laser profilometer, CT scan, and photogrammetry techniques were all attempted to acquire the original rock sample fracture surface. The profilometer takes about two hours to scan the surface of the fracture conductivity sample at a 0.05 inch measurement interval. The profilometer stores data in text format which loses resolution while converting the fracture surface data to stereolithography format. The CT scan takes a relatively shorter time of about 15 minutes per sample fracture face and gives a whole sample scan but is expensive. These scans are processed with software such as ImageJ and Slicer to get an appreciable image. The photogrammetry takes about 10 minutes per sample fracture face but a relatively long time to process images with software like Meshroom.

The print time of the required 3D model is typically long and would have to be restarted from scratch if any error or technical challenge is encountered during printing. Confirm 3D models to be printed before starting. Check printer nozzle and ensure correct diameter, and sufficient filament rolls (if using FDM printer). Do not print in very bright rooms (when using a DLP printer).

The fracture conductivity replicate samples are relatively weaker than the original samples in terms of compressive strength. The conventional fracture conductivity testing axial stress range (1000 to 4000 psi) was modified. Triaxial experiments were tested on artificially made core plugs with similar composition as the replicate samples.

Prepping the replicates for fracture conductivity testing was also a major challenge. The epoxy did not bind to the cement replicates well. The high porosity of these cement replicates allowed epoxy to infiltrate and damage the samples. The replicate samples were coated with cement sealant and were taped all around using construction/gorilla glue to aid adhesion before epoxying samples. Replicates were also allowed to cure for some days.

3. DISCUSSION OF RESULTS

3.1 Introduction

This chapter discusses the experimental fracture conductivity results of testing fractured rock replicates. These fracture conductivity samples are replicated using 3D printing technology as discussed in the previous chapter. The replicates are also validated by visual comparisons, JRC estimates, and fracture conductivity results. Mechanical properties of the replicate samples are also estimated from conventional triaxial tests on core plugs.

3.2 Visual Comparisons

The scanned data using the laser profilometer can be plotted and analyzed using the MATLAB code developed by (Nieto, 2007). We used a measurement interval of 0.05 in. This interval is also suitable for the Tse & Cruden, (1979) correlation of the Z_2 parameter and JRC. The 3-dimensional fracture surface profile is used as a first pass at replicability check.

The following Figures 3-1 to 3-9 show visual comparisons of the scanned fracture surfaces. Two different fractured cores, Meremac and Austin chalk were scanned using the laser profilometer. Fig 3-1 compares the original Mermac core and the 3D mold printed with Digital Light Processing. Figs 3-2 to 3-5 show comparisons between the replicates and the original Meremac. These figures show good similarities based on visual analysis because both halves of the original Meremac core were relatively mated. The Digital Light Processing is also an advantage to replicating the details of the fracture surface.

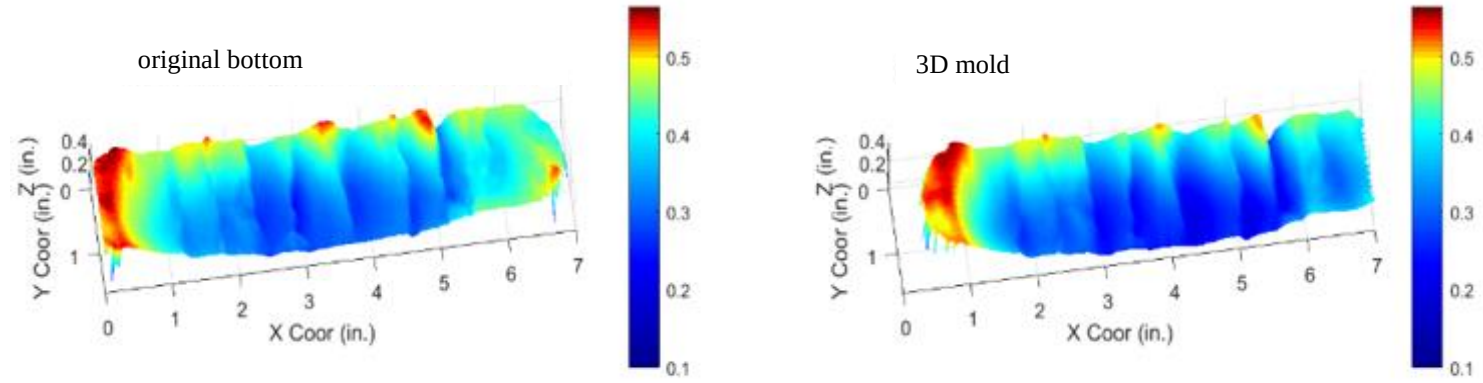

Figure 3-1: surface scan of original Meremac core and 3D printed mold

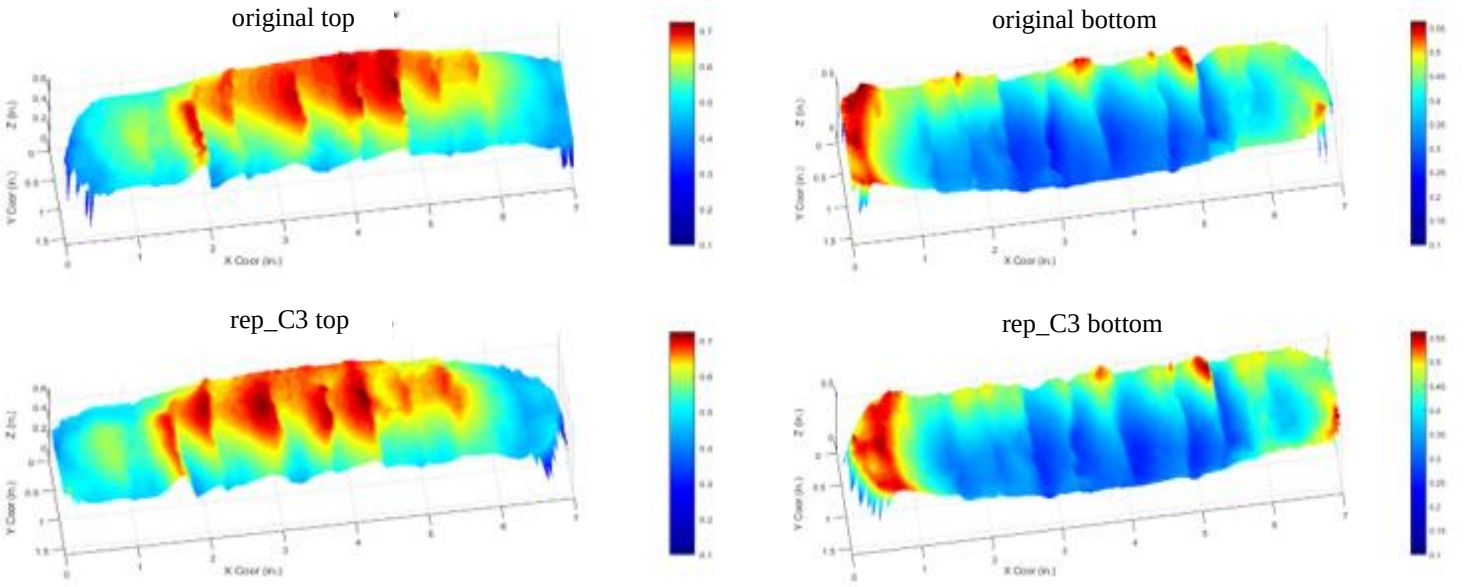

Figure 3-2: surface scan of original Meremac core (top and bottom) and concrete replicate_C3 (top and bottom)

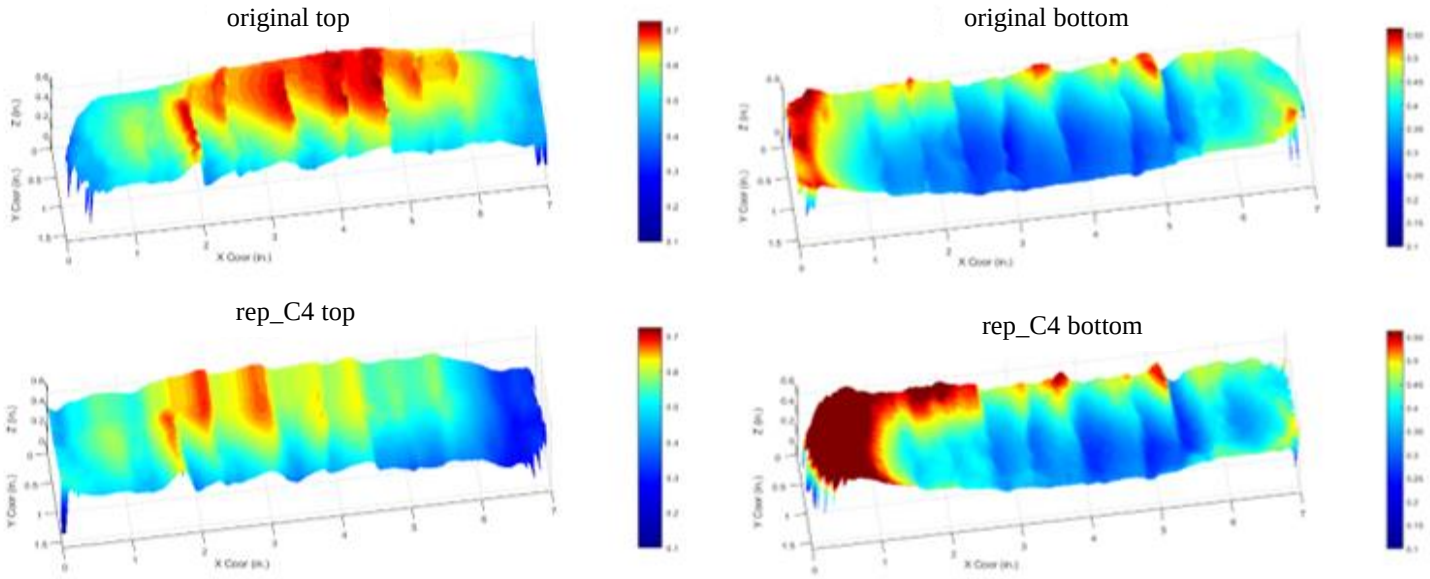

Figure 3-3: surface scan of original Meremac core (top and bottom) and concrete replicate_C4 (top and bottom)

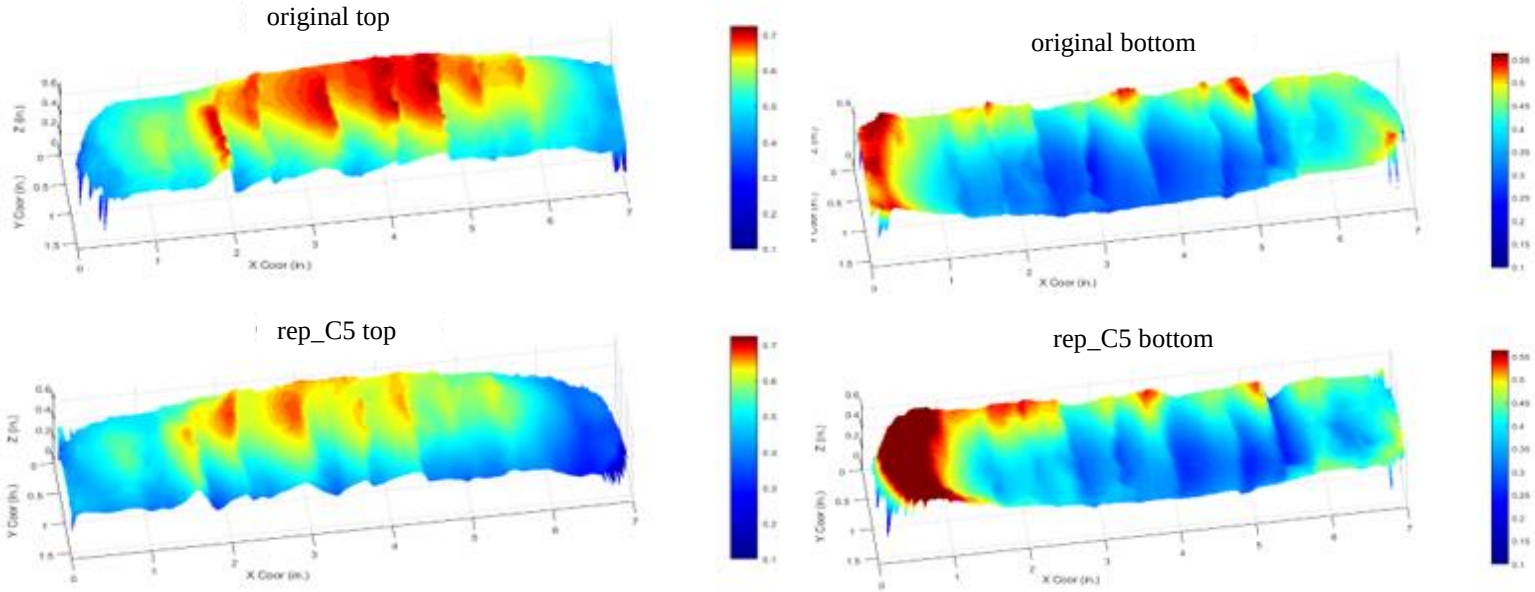

Figure 3-4: surface scan of original Meremac core (top and bottom) and concrete replicate_C5 (top and bottom)

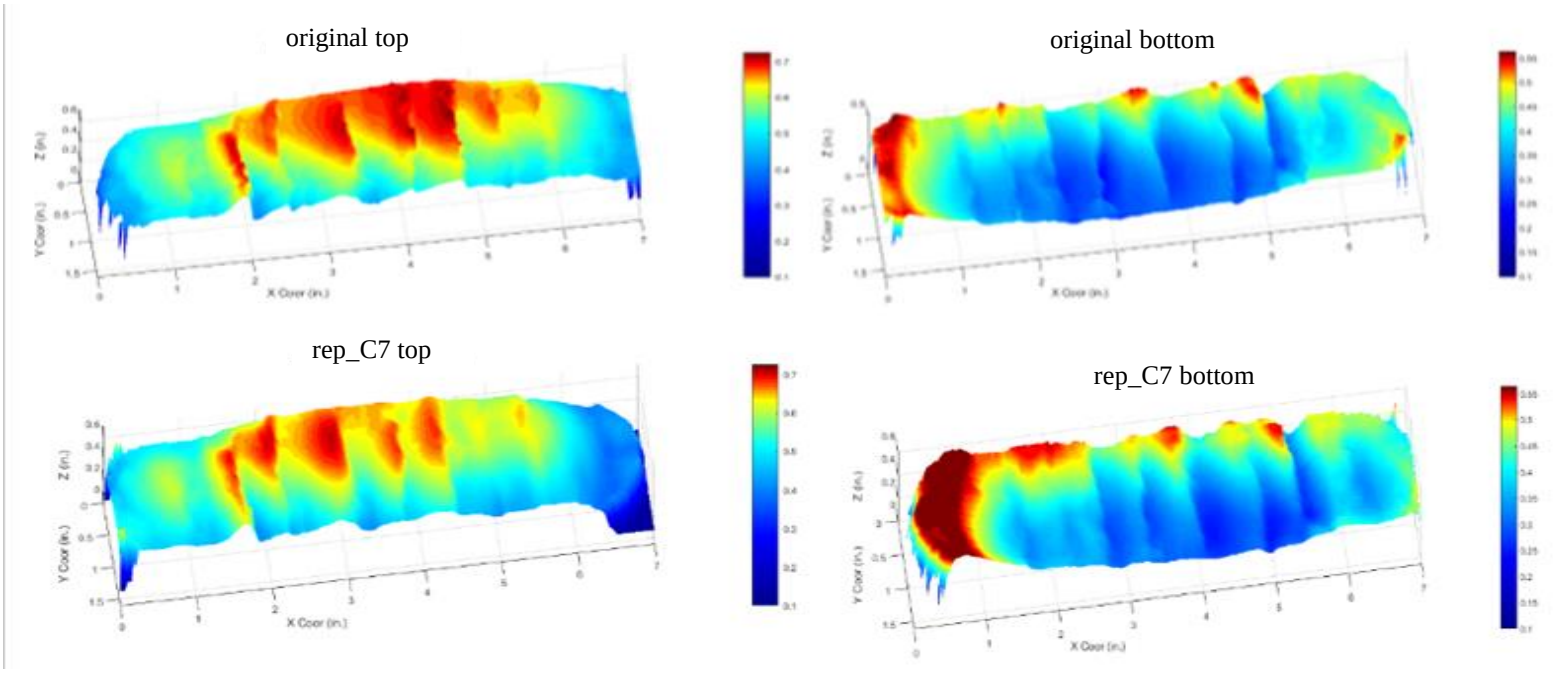

Figure 3-5: surface scan of original Meremac core (top and bottom) and concrete replicate_C7 (top and bottom)

Fig 3-6 compares the original Austin Chalk core and the 3D mold printed with Fused Deposition modeling. Figs 3-7 to 3-9 show comparisons between the replicates and the original Austin Chalk core. These figures do not show very matching similarities based on visual analysis because both halves of the original Austin Chalk core were relatively not mated. The bottom replicates show better similarity than the top because the 3D mold was printed from scans of the original bottom half. The combination of the photogrammetry technique with Fused Deposition Modeling is another possible reason why replicability is reduced. The Fused Deposition Modeling made a "finger print" pattern on the fracture surface due to the filament (Polylactic acid) deposition.

original top

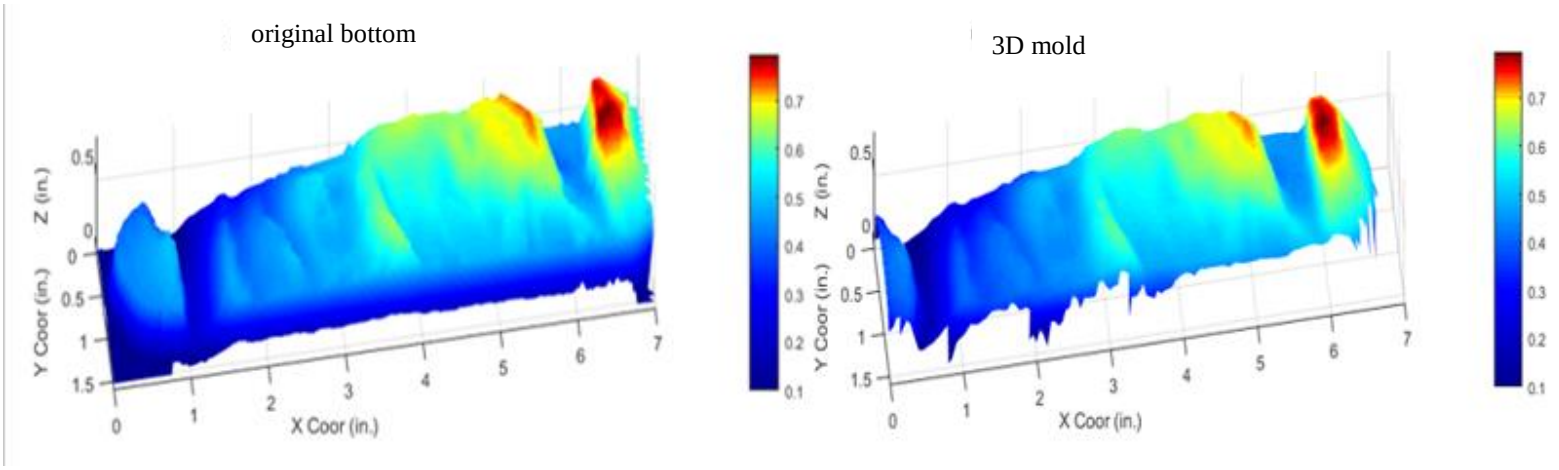

Figure 3-6: surface scan of original Austin chalk core (top) and 3D printed mold (top)

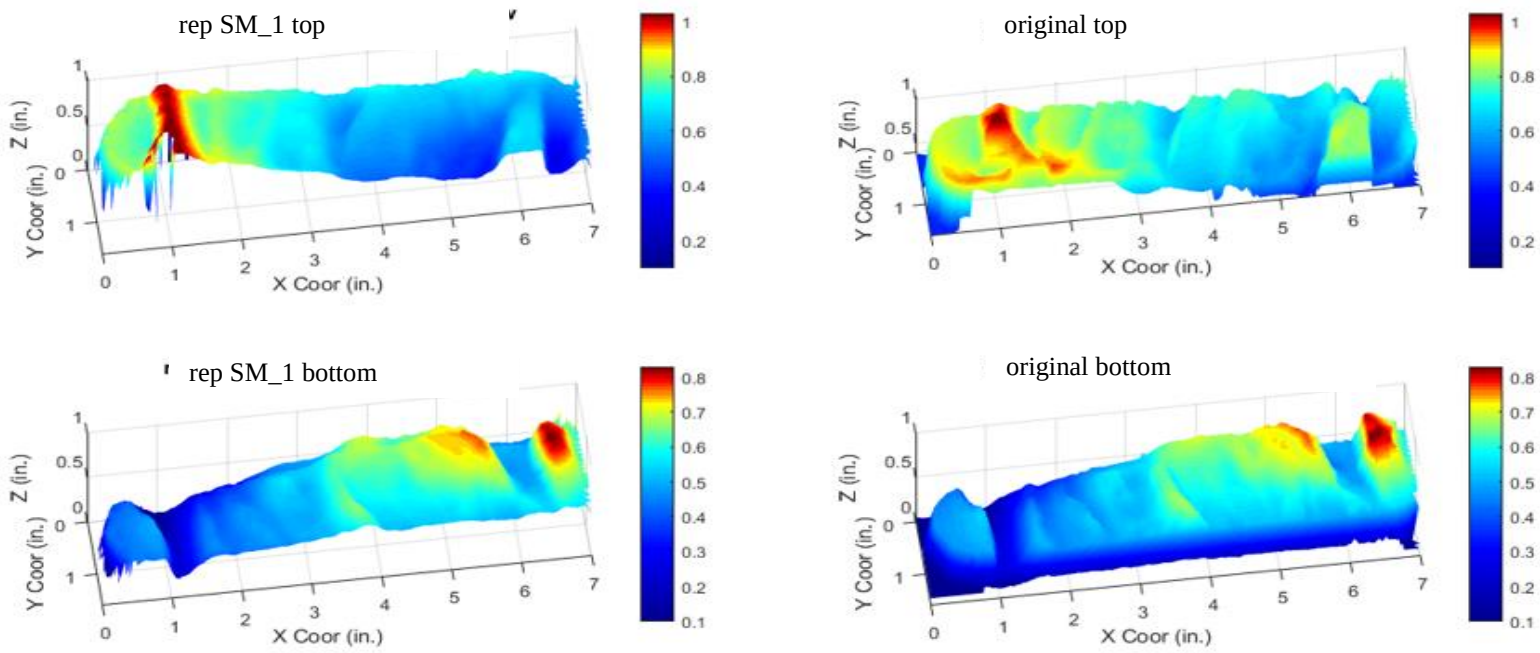

Figure 3-7: surface scan of original Austin chalk core (top and bottom) and concrete replicate_SM_01 (top and bottom)

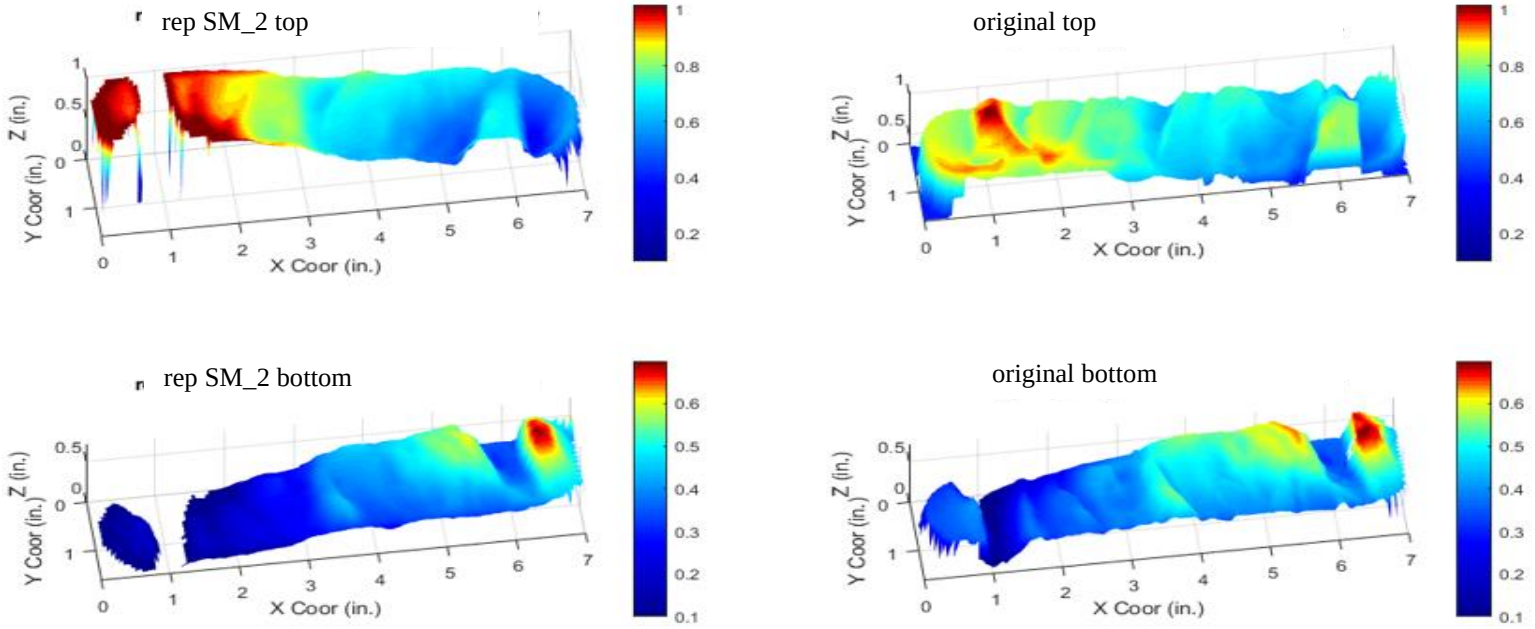

Figure 3-8: surface scan of original Austin chalk core (top and bottom) and concrete replicate_SM_02 (top and bottom)

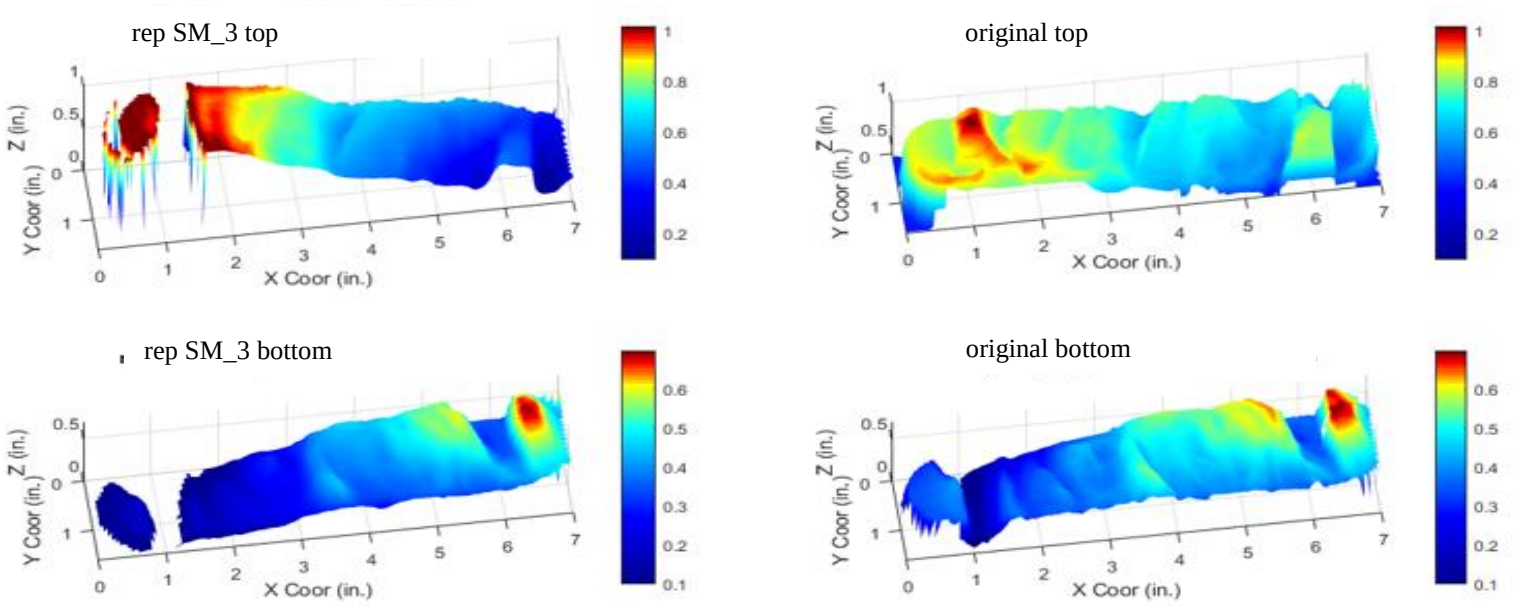

Figure 3-9: surface scan of original Austin chalk core (top and bottom) and concrete replicate_SM_03 (top and bottom)

3.3 Joint Roughness Coefficient Estimate

For this study, we use the root-mean-square of the surface profile's first derivative the Z_2 parameter to estimate the JRC. The relationship between Z_2 and JRC developed by (Tse & Cruden, 1979) is used to estimate the roughness in this study. This is because **Eq. 3.2** is developed based on a measurement interval of 1.27mm (0.05inch) similar to the measurement interval of our profilometer. The Z_2 and JRC used in this study are stated here again as **Eq. 3.1** and **Eq. 3.2.**

$$Z_2 = \left[\frac{1}{L}\sum_{i=1}^{n-1}\frac{(z_{i+1}-z_i)^2}{x_{i+1}-x_i}\right]^{\frac{1}{2}} \qquad 3.1$$

$$JRC = 32.3 + 32.47\log(Z_2) \qquad 3.2$$

The Z_2 is measured by reading height values (z-axis from profilometer data) along with the intervals as shown in the fig below. For the fracture conductivity sample size, there are about 141 intervals along the sample length and 35 intervals along the sample width. The extracted profiles along the surface are used to obtain a mean Z_2. The mean Z_2 is then used to estimate the JRC.

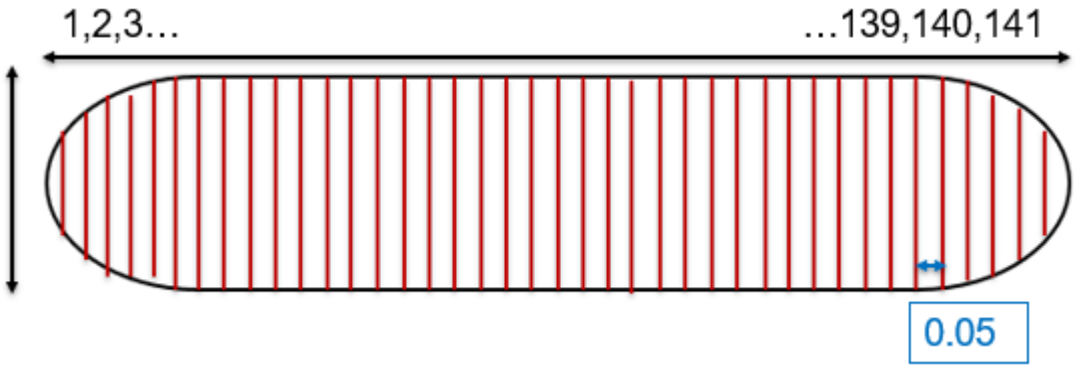

Figure 3-10: profile location on a scanned rock sample

Table 2: Z_2 values and JRC estimates for Meremac cores

Core	Z_2	JRC
original _bt	**0.532**	**23.304**
mold_bt	**0.540**	**23.502**
C3_bt	0.554	23.870
C4_bt	0.735	27.870
C5_bt	0.533	23.310
C7_bt	0.494	22.260
C9_bt	0.536	23.400

Core	Z_2	JRC
original_tp	0.496	22.309
C3_tp	0.519	22.938
C4_tp	0.502	22.476
C5_tp	0.432	20.354
C7_tp	0.427	20.183
C9_tp	0.373	18.274

Table 3: Z_2 values and JRC estimates for Austin chalk cores

Core	Z_2	JRC
original_bt	**0.620**	**25.460**
SM mold_bt	**0.592**	**24.813**
SM_01_bt	**0.550**	23.770
SM_02_bt	0.528	23.194
SM_03_bt	0.396	19.154

Core	Z_2	JRC
original_tp	**0.626**	**25.595**
SM_01_tp	0.939	31.308
SM_02_tp	0.909	30.858
SM_03_tp	0.917	30.980

The Joint Roughness Coefficient of the original Meremac and Austin Chalk cores were computed with **Eq. 3.2**. The JRC of their respective 3D molds and replicates were also computed to quantify the roughness and compare replicability. These results are presented in Table 2 and Table 3 for the Meremac and Austin Chalk samples respectively. The Meremac replicates show replicability ranging from 78% to 99% when compared to the original Meremac sample. The Austin Chalk replicates show replicability ranging from 75% to 93% when compared to the original Austin Chalk sample. The original Austin Chalk sample was highly fractured with difference in positive and negative peaks greater than 0.5 inch. The original Austin Chalk sample was also not mated as the original Meremac. These combined effects explain the variation in JRC values shown in Table 2 and Table 3. The Austin Chalk top replicates show significant increase in JRC relative to the original. This is because of the additional

artificial fracture surfaces created on the replicates due to the non-mated original sample. Based on the computed JRC for each core, the Meremac samples show a better replicability than the Austin Chalk samples. This supports the comparison by visual analysis.

3.4 Fracture Conductivity Tests

Here we discuss the results from the fracture conductivity test of the concrete replicates. Two different cores were replicated, a Meremac core (sample No. 2) from Copeland, (2020) and a fractured Austin chalk core. Fracture conductivity estimates for the original Meremac core are available in Copeland, (2020). The fractured Austin chalk core does not have fracture conductivity results for the original rock. All concrete replicates were loaded in closure stress ranging from 100 psi to 4000 psi although most replicates could only produce results up to 2000 psi. This study used a 0.2 lbm^2 /ft proppant concentration similar to (Copeland, 2020).

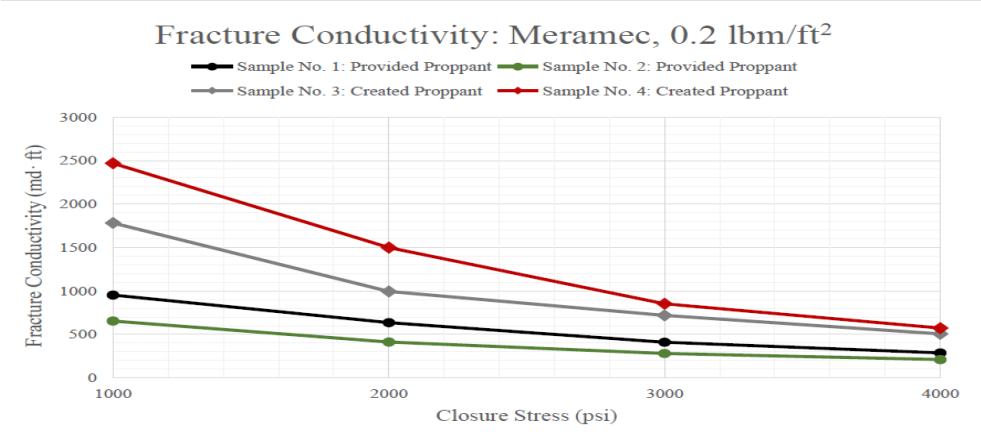

Figure 3-11: fracture conductivity result from original Meremac core (Copeland, 2020)

The first concrete replicate C1 was a mixture of cement and shale. Sample C1 had a curing time of more than 6 days. The top and bottom of C1 were cast at about 1.5 in and the remaining

height was made up of sandstone spacers. These spacers increased the strength of C1 relative to other samples. A single fracture conductivity value of 248 md-ft was estimated at closure stress of 1000 psi on the first attempt. Further testing of C1 was stopped because the epoxy layer on the sample limited the effect of the closure stress on C1. The integrity of the sample C1 was still intact so we prepped C1 again with the same spacer for a second test.

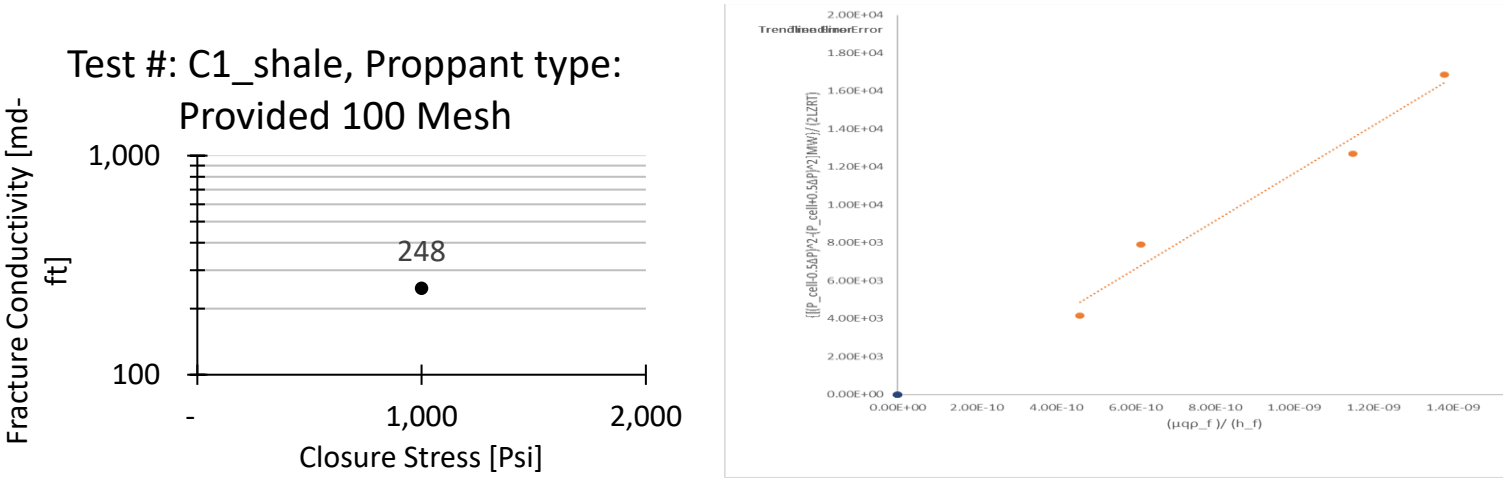

Figure 3-12: fracture conductivity result from C1_test 1 (Meremac replicate, shale with spacer)

The second test of C1 was started at a closure stress of 500 psi since the strength of the concrete replica/spacer (C1) was unknown. We were able to get three conductivity points for this test. The results are shown in the fig below. The concrete in the top half of sample C1 was split into two upon opening the sample.

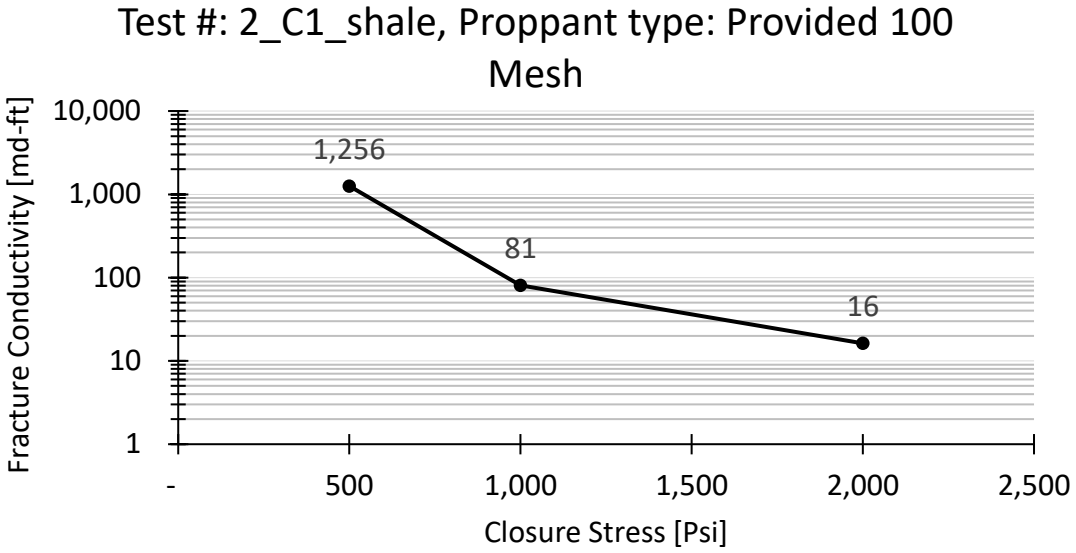

Figure 3-13: fracture conductivity result from C1_test 2 (Meremac replicate, shale with spacer)

The concrete replicate C2 was also a mixture of cement and shale. The bottom and top half of Sample C2 had a difference in curing time of about 2 days. The top cured relatively longer than the bottom for about 6 days. The bottom half was cast with relatively wetter shale cuttings than the top half. The top and bottom of C2 were cast entirely with the cement/shale mixture.

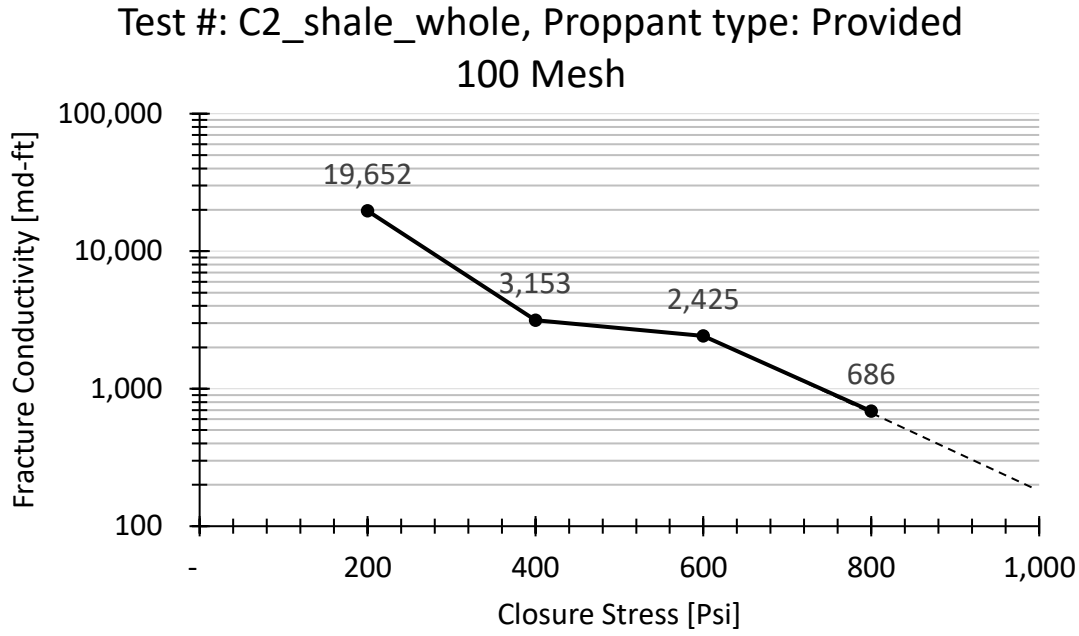

Figure 3-14: fracture conductivity result from C2 (Meremac replicate, entirely shale)

The concrete replicate C3 was also cast entirely of cement and shale. Visual comparison of the replicate C3 and the original rock are shown in **Fig 3-2.** Both bottom and top half cured for about three days, with a difference in curing time of about 6hrs. closure stress ranging from 100 psi to 2000 psi was used because of the expected weak nature of the replicate. The stress displacement behavior was also monitored during the experiment. This has been color-coded with the fracture conductivity results from the experiment. We believe the true fracture conductivity of this experiment is beyond the red region which has a relatively constant slope on the stress-displacement graph.

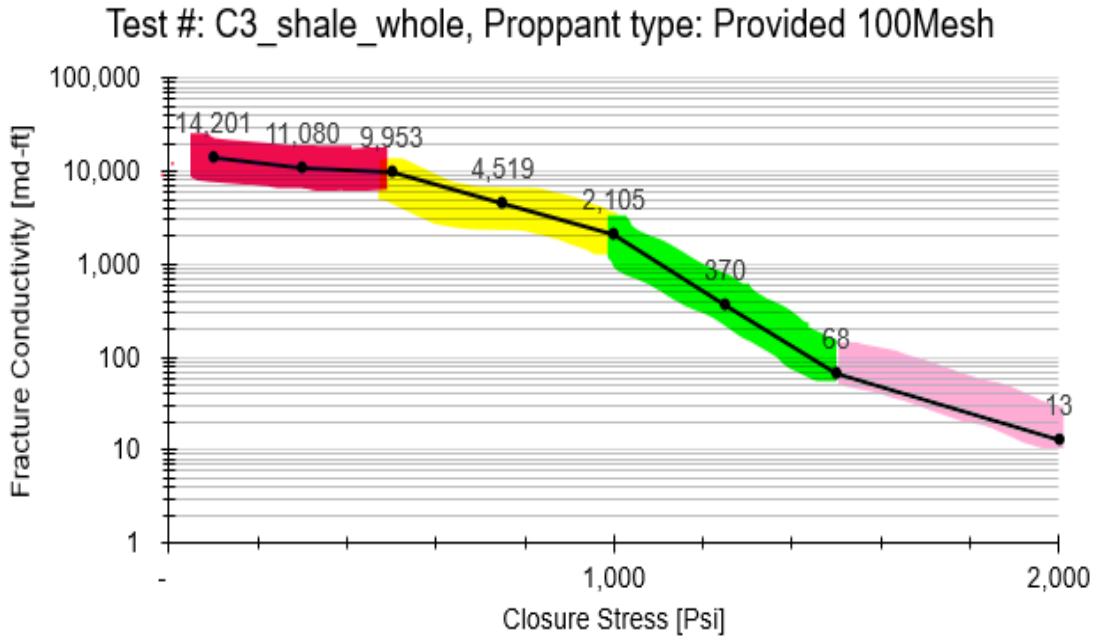

Figure 3-15: fracture conductivity result from C3 (Meremac replicate, entirely shale)

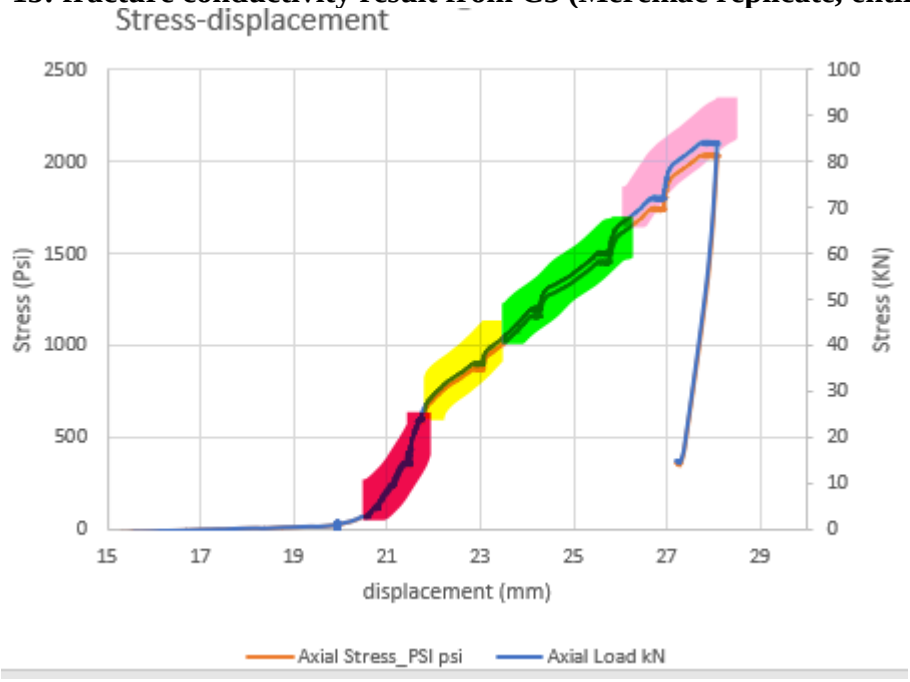

Figure 3-16: stress-displacement curve during C3 test

The concrete replicate C4 was cast entirely of cement and sand. Visual comparison of the replicate C4 and the original Meremac core are shown in **Fig 3-3.** Both bottom and

top half cured for about three days, with a difference in curing time of about 6 hrs. Closure stress ranging from 100 psi to 2000 psi was also used because of the expected weak nature of the replicate. The stress displacement behavior was also monitored during the experiment as shown in **Fig 3-16**. Core plugs were also made with the concrete batch from the C3 and C4 samples to test for their mechanical properties. The results of the uniaxial compressional strength test are reported in the succeeding section.

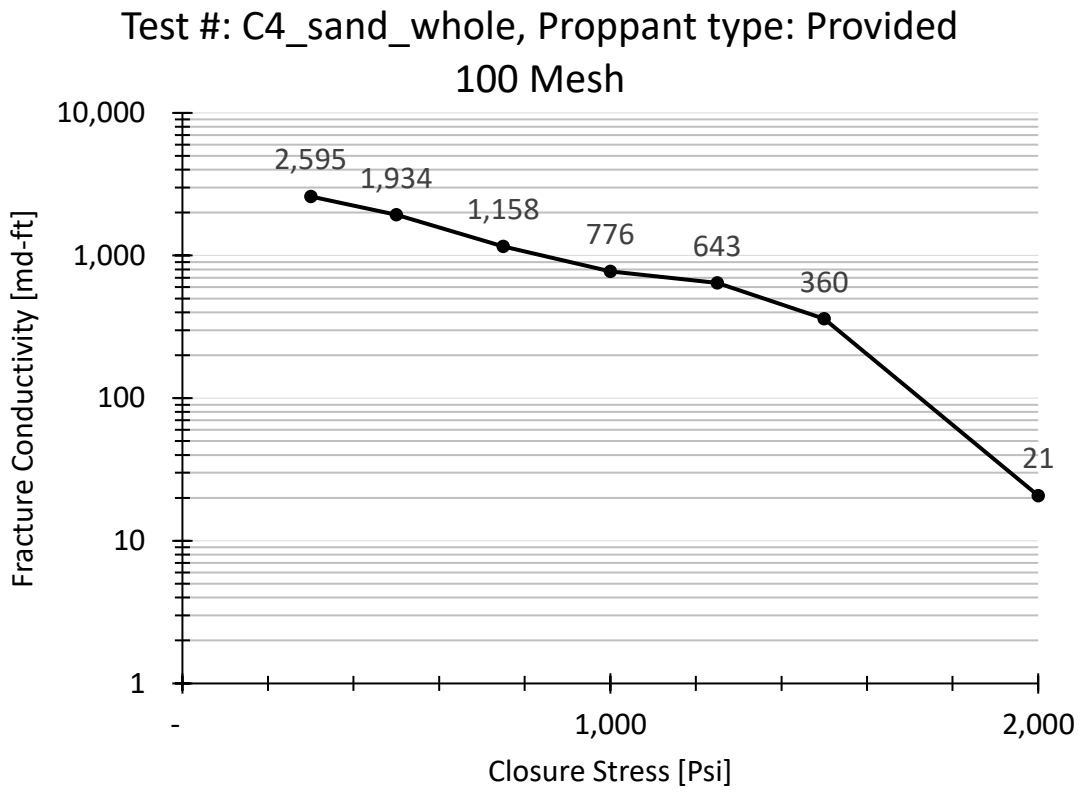

Figure 3-17: fracture conductivity result from C4 (Meremac replicate, entirely sand)

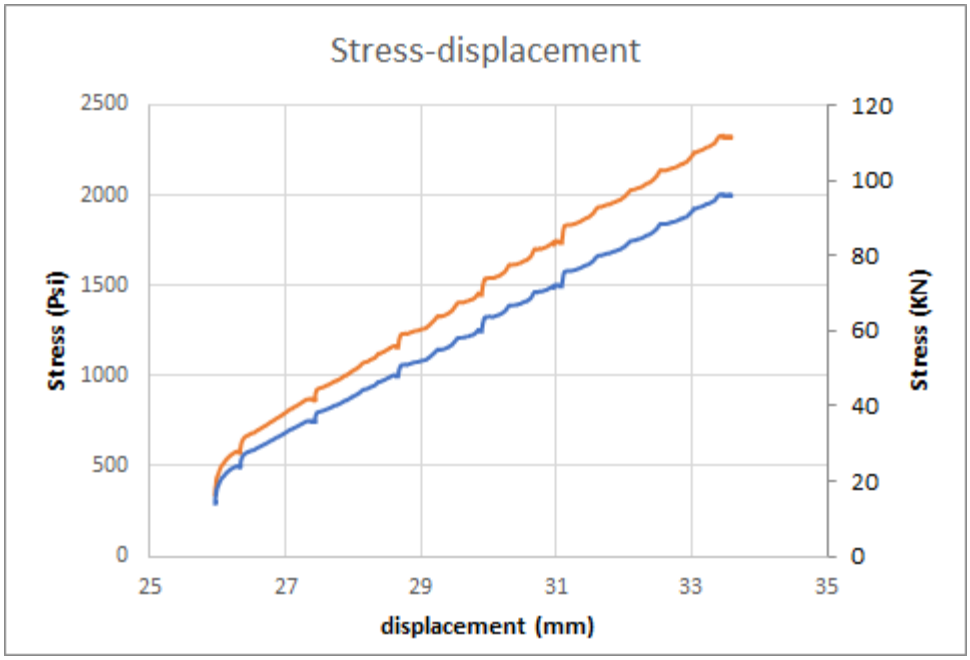

Figure 3-18: stress-displacement curve during C4 test

The concrete replicates C5 and C7 were cast entirely of cement and sand with relatively similar curing time and treating conditions. Visual comparison of the replicates C5 and C7, and the original Meremac core are shown in **Fig 3-4** and **Fig 3-5** respectively**.** They were both soaked in acetone and brushed to clean off the grease used as a release agent during casting. They were also both coated with cement sealant to preserve the integrity of the replicates when epoxying them. Both bottom and top half of both samples cured for about three days, with a difference in curing time of about 4 hrs. Closure stress ranging from 300 psi to 1500 psi was tested for fracture conductivity. The stress displacement behavior was also monitored during the experiment. Replicate C5 and C7 showed great replicability based on the results as shown in **Fig 3-19**. Based on these results, it is evident that the true fracture conductivity behavior of these samples can be

tested between 750 psi and 1500 psi. This is akin to the peak strength of the cement/sand core which ranges from about 1000 psi to 1400 psi for 3 days cured sample.

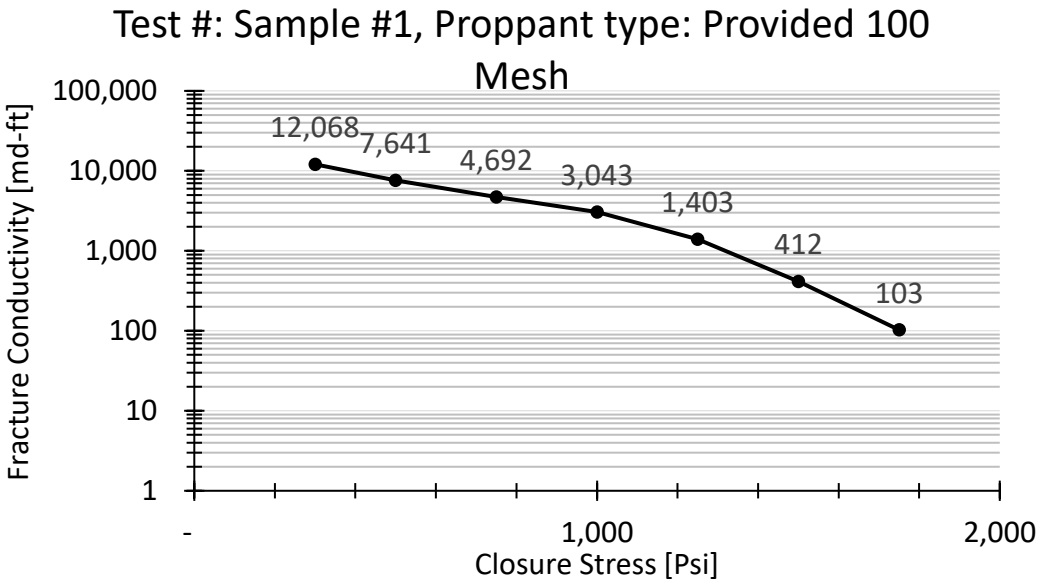

Figure 3-19: fracture conductivity result from C5 (Meremac replicate, entirely sand)

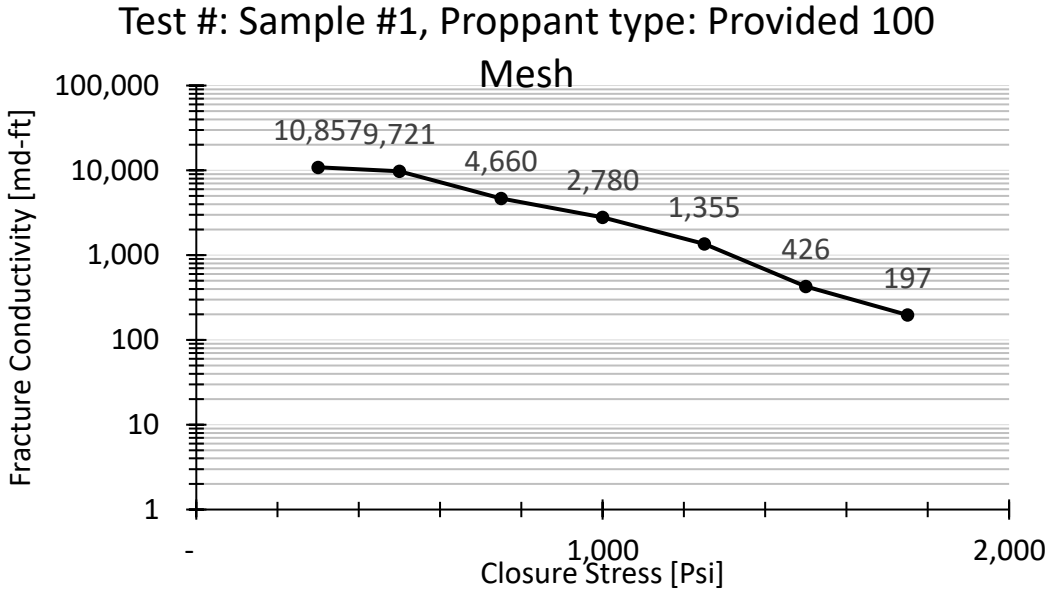

Figure 3-20: fracture conductivity result from C7 (Meremac replicate, entirely sand)

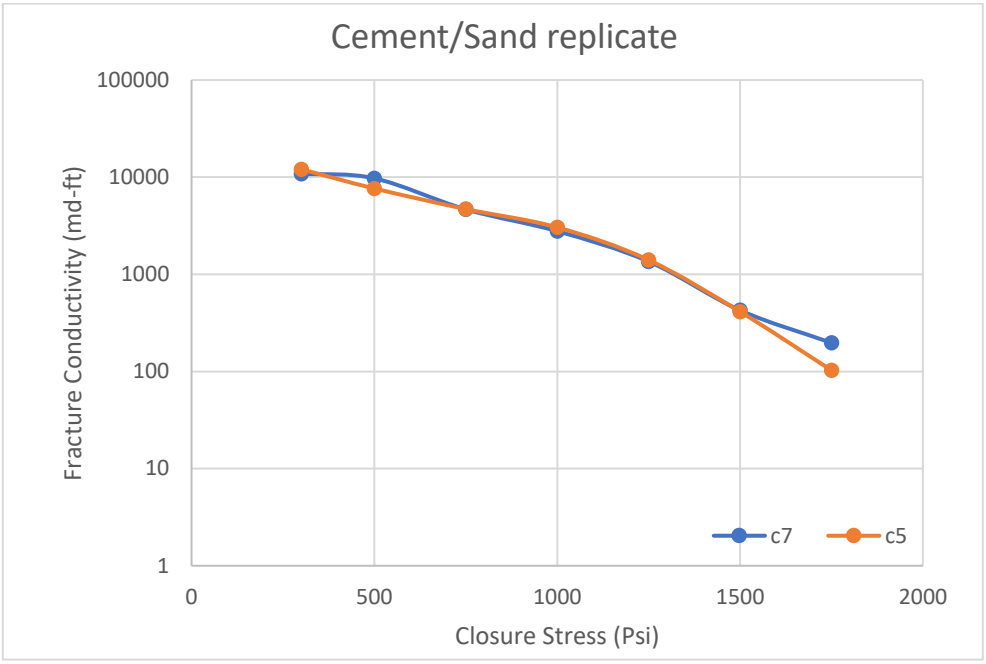

Figure 3-21: fracture conductivity result from C5 and C7 tests

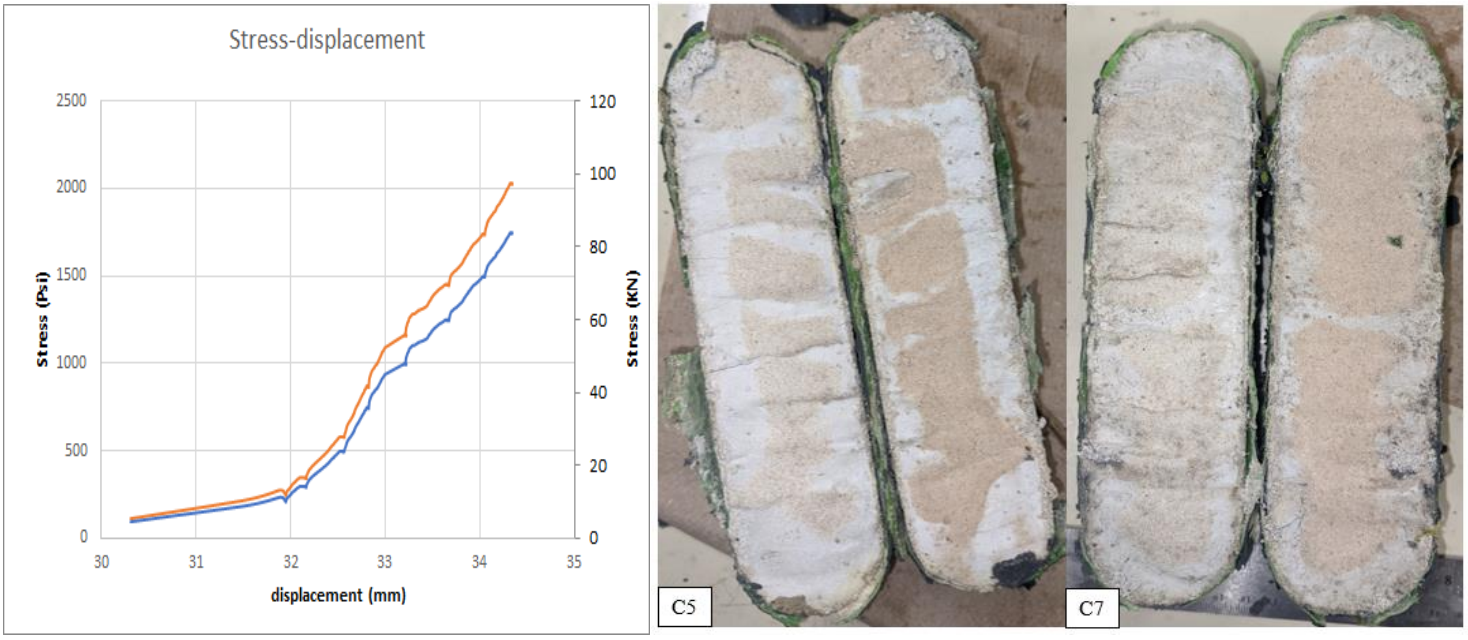

Figure 3-22: stress-displacement curve during C7 test (left), replicates C5 and C7 after testing (right).

Fractured Austin chalk was also replicated to validate the proposed workflow. The concrete replicate C8 was cast entirely of cement and sand. Both bottom and top half cured for about three days, with a difference in curing time of about 6hrs. closure stress ranging from 300 psi to 1500 psi was also used. The stress displacement behavior was also monitored during the experiment. The Austin chalk sample was significantly fractured with one end of the sample dominantly high and the other end low. The changing high and low caused the fracture not to line up with the cell pressure port and a differential sensor port. We slightly chipped off the edge of the fracture side not matching up to allow gas flow to the port thus noticeable pressure readings on the sensors.

Figure 3-23: original fractured Austin chalk sample

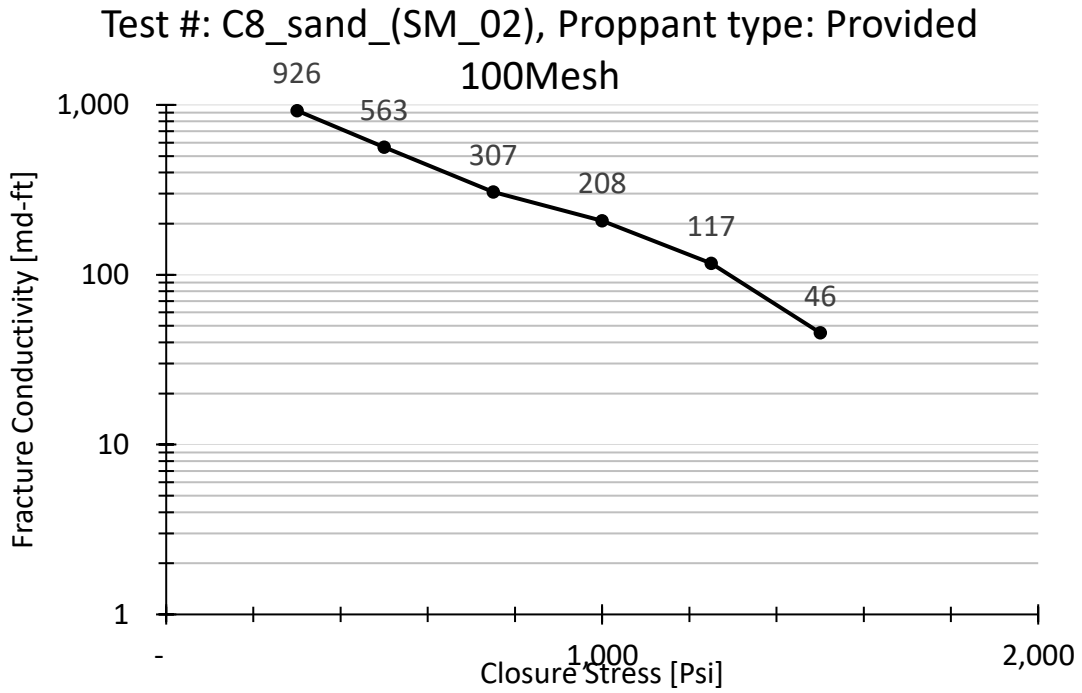

Figure 3-24: fracture conductivity result from C8 (Austin chalk replicate, entirely sand)

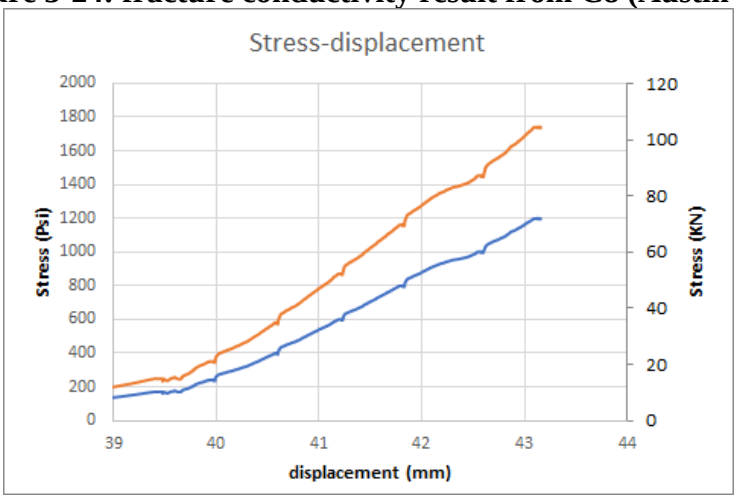

Figure 3-25: stress-displacement curve during C8 test

3.5 Unconfined Compressive Strength Tests

Using 3D printed molds, we cast core plugs of 1.0 in diameter. These cores were then cut and ground to a length of about 2.25 in. 5 unconfined compressive strength (UCS)

tests were performed with these cores at a rate of about 6 micron/s with a Large Sample Rig (LSR) in the Handin rock deformation lab.

Figure 3-26: Core plugs for UCS (left), Large Sample Rig equipment for UCS (right)

The samples were jacketed twice with polyolefin heat shrinks, with light grease on top and bottom core face to reduce friction effects. Two of the samples (C4_A, C4_B) are cement/sand mixtures while 3 (C2, C3_A, C3_B) are cement/shale mixtures. The results from the UCS test show that the cement/sand mixture is relatively stronger than the cement/shale mixture. The charts and table below show the stress-strain curve and the strength respectively of the cores from the UCS test.

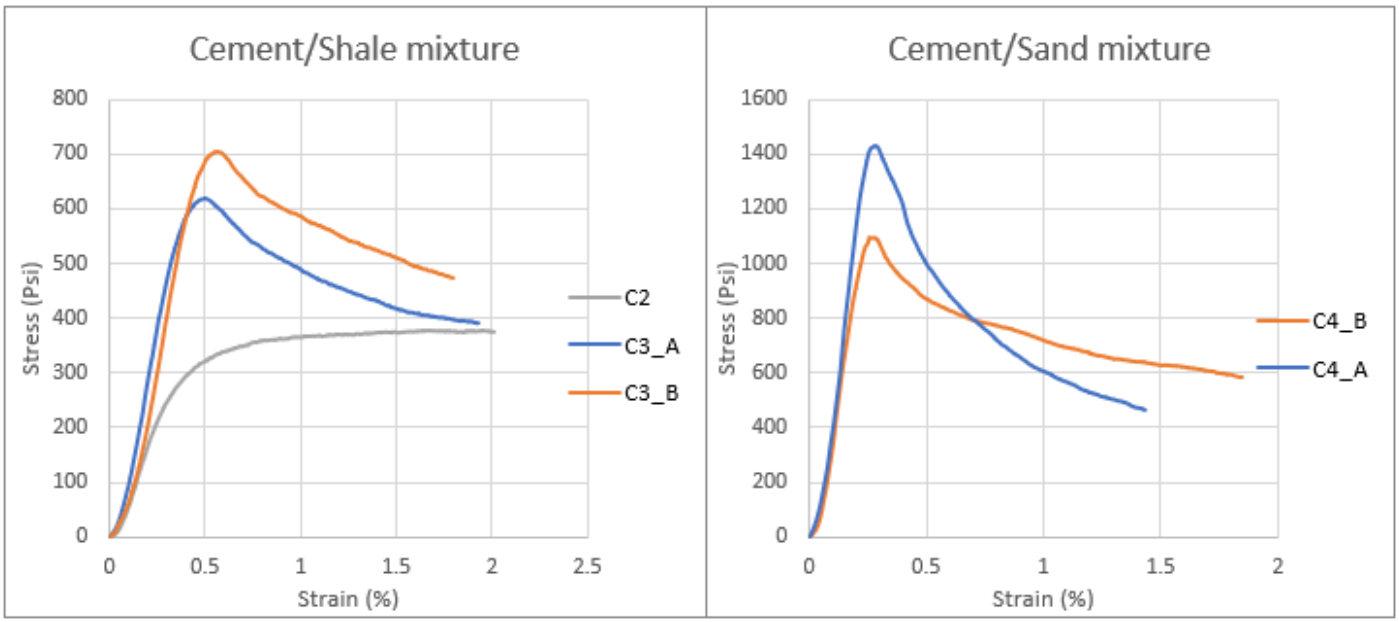

Figure 3-27: stress-strain curves from UCS test

Table 4: Summary of results from UCS test

Core	**Young's modulus (Psi)**	**Peak Strength (Psi)**	**composition**
C2	961	379	
C3_A	1953	621	cement/shale
C3_B	2007	703	
C4_A	7798	1430	
C4_B	6328	1095	cement/sand

4. CONCLUSIONS AND RECOMMENDATIONS

4.1 Conclusions

This thesis presents a workflow to replicate the fracture surface topography and achieve consistency of fracture conductivity samples. This will provide valuable insights into experimental studies on hydraulic fracturing. The effects of surface topography, proppant distribution, grain size distribution, fluid carrying ability of fracturing fluids on fracture conductivity can be qualitatively investigated now.

For this study, we have used a laser profilometer, CT scans, and photogrammetry techniques to acquire fracture surface data. We generated 3D models of the original rocks and replicated samples using digital light processing and fused deposition modeling 3D printers. Replicability was validated by visual comparisons of fracture surfaces, using the joint roughness coefficient estimate and results from fracture conductivity testing.

Based on this, we state the following conclusions:

1. 3D printing can be applied for fracture conductivity testing to replicate fracture surfaces and experimentally investigate factors that contribute to fracture conductivity.
2. Mechanical properties and surface topography of rock samples dominate fracture conductivity behavior especially at closure stress within the peak strength of the rock sample.

3. For detailed fracture surface replicability, the digital light printer (DLP) is relatively more preferred than the fused deposition modeling printer. This is vice versa for print jobs that require stronger 3D prints.

4.2 Limitations, Recommendations, and Future Work

The study of the replicability of these samples is mainly limited by time. The strength of these replicates increases with additional curing time. Another factor that limited this study is the availability of original rock samples with significant fracture surface topography and fracture conductivity results of these original rocks for comparisons.

We recommend that the following be considered for future work:

1. Replicate samples with several samples with relatively similar curing conditions and for different curing times. The strength of these replicates increases geometrically with curing time.
2. Samples should be kept moisturized (spray with water) throughout the intended curing time and dried at a temperature just below boiling point to terminate curing. Curing is a continuous chemical reaction that needs water to go on.
3. The top and bottom halves of the sample for fracture conductivity testing should be made as close as possible. If using a quick setting cement and a single mold, a 4hr difference in cast time is optimal. Use two different molds of each half and cast both together for optimal consistency. Core plugs from each set of replicates should also be made for testing mechanical properties.

4. Use the laser profilometer to acquire fracture surface first. This is the most detailed but loses its advantage when converting text files to STL format. Use the CT scan when the fracture surface has many undulating points. Photogrammetry is relatively easier and faster in capturing surfaces but takes time to render an image and produce a 3D model.
5. When using photogrammetry do not capture images in areas with reflective surfaces, add colors in the background for more details. Use the DLP when fracture surface requires more detail and the FDM for molds that need strength more in terms of functionality.
6. For future work, factorial design can be used for experiments with several replicated samples. This can be used to modify existing fracture conductivity correlations based on both qualitative and quantitative studies of parameters that affect fracture conductivity.

REFERENCES

AliceVision. (2021). *https://alicevision.org/#meshroom.* Retrieved from https://alicevision.org.

Al-Tahini, A., Sondergeld, C., & Rai, C. (2006). The Effect of Cementation on the Mechanical Properties of Sandstones. *SPE Reservoir Evaluation & Engineering, 9(4)*, 308-316.

API-RP-61. (1989, October 1). Recommended Practices for Evaluating Short Term Proppant Pack Conductivity. *First*. Washington, D.C, U.S.A: American Petroleum Institute.

ASTM-Standard-D7012-14. (2014). Standard Test Methods for Compressive Strength and Elastic Moduli of Intact Rock Core Specimens Under Varying States of Stress and Temperatures. West Conshohocken, Pennsylvannia, USA: ASTM International.

Awokele, O. (2013). *Dynamic Fracture Conductivity- An Experimental Investigation Based on Factorial Analysis.* Ph.D. Dissertation, Texas A&M University, Petroleum Engineering, College Station.

Awoleke, O., Zhu, D., & Hill, A. (2016). New Propped-Fracture Conductivity Models For Tight Gas Sands. *SPE Journal*, 1,508-1,517.

Barree, R., & Duenckel, R. (2019). The limits of Fluid Flow in Propped Fractures- the Disparity Between Effective Flowing and Created Fracture Lengths. *SPE Hydraulic Fracturing Technical Conference.* The Woodlands, Texas, USA: SPE-194355-MS.

Barton, N., & Choubey, V. (1977). The Shear Strength of Rock Joints in Theory and Practice. *Rock Mechanics*, 1-54.

Burns, M., & Wangenheim, C. (2019). Metal 3D Printing Applications in the Oil & Gas Industry. *SPE-1947878-MS*.

Camisa, J., Verma, V., Marler, D., & Madlinger, A. (2014). Additive Manufacturing and 3D Printing for Oil and Gas - Transformative Potential and Technology Constraints . *International Ocean and Polar Engineering Conference* (pp. 299-306). Busan, Korea: ISOPE.

Cooke Jr, C. (1973). Conductivity of Fracture Proppants in Multiple Layers. *Journal of Petroleum Technology*, 1101-1107.

Copeland, A. (2020). *The Impact of Proppant Grain-Size Distribution on Fracture Conductivity in Shale Formations.* Texas A&M University, Petroleum Engineering, College Station.

Craig, D., Barree, R., Warpinski, N., & Blasingame, T. (2017). Fracture Closure Stress: Reexaminig Field and Laboratory Experiments of Fracture Closure Using Modern Interpretation Methodologies. *Society of Petroleum Engineers*(SPE-187038).

Elsarawy, A., & Nasr-El-Din, H. (2018). Propped Fracture Conductivity in Shale Reservoirs: A Review of its Importance and Roles in Fracturing Fluid Engineering. *SPE-192451-MS*.

Enriquez, O. (2016). *A Comprehensive Study of the Eagle Ford Shale Fracture Conductivity.* Thesis, Texas A&M University, Petroleum Engineering, College Station.

Enriquez, O., Knorr, A., Zhu, D., & Hill, A. (2016). Relationships between Mechanical Properties and Fracturing Conductivity for the Eagle Ford Shale. *Society of Petroleum Engineers*.

Guerra, J. (2019). *Fracture Conductivity Behavior in Shale Formations.* Thesis, Texas A&M University, Petroleum engineering, College station.

Gupta, A., Rai, C., & Sondergeld, C. (2019). Experimental Investigation of Propped Fracturre Conductivity and Proppnat Diagenesis. *URTec:363*.

Isleyen, E., & Duzgun, H. (2018). Evaluation of 3D Printing in Obtaining Replicates of Discontinuity Roughness. *ARMA 18-0015*.

Jang, H., Kang, S., & Jang, B. (2014). Determination of Joint Roughness Coefficients Using Roughness parameters. *Rock Mechanics and Rock Engineering*, 2061-2073.

Jiang, C., Zhao, G., Gao, M., & Zhao, Y. (2016). A Trial of 3D printing on Rock Dynamics. *Rock Dynamics: From Research to Engineering*.

Jiang, Q., Feng, X., Song, L., Gong, Y., & Zheng, H. C. (2015). Modeling rock specimens through 3D printing: Tentative experiments and prospects. *Springer*, 101-111.

Kamali, A., & Pournik, M. (2015). An Investigation of Rough Surface Closure with Application to Fracturing. *ARMA*.

Kulatilake, P., Balasingham, P., Park, J., & Morgan, R. (2006). Natural rock joint roughness quantification through fractal techniques. *Geotechnical and Geological Engineering*, 1181-1202.

Li, L., & Aubertin, M. (2003). A general relationship between porosity and uniaxial strength of engineering materials. *Canadian Journal of Civil Engineering, 30(4),* 644-658. doi:https://doi.org/10.1139/l03-012

Maerz, N., Franklin, J., & Bennett, C. (1990). Joint roughness measurement using shadow profilometry. *International Journal of Rock Mechanics and Mining Sciences*, 329-343.

Marpaung, F. (2007). *Investigation of The Effect of Gel Residue on Hydraulic Fracture Conductivity Using Dynamic Fracture Conductivity Test.* Thesis, Texas A&M University, Petroleum Engineering, College Station, Texas.

Miskimins, J. (2019). *Hydraulic Fracturing Fundamentals and Advancements.* Societ of Petroleum Engineers.

Mittal, A., Rai, C., & Sondergeld, C. (2017). Laboratory Investigation of Proppant-Pack Conductivity: Eagle Ford and Vaca Muerta Shale. *URTec*. doi:10.15530/URTEC-2017-2670951

Mittal, A., Rai, C., & Sondergeld, C. (2018). Proppant-Conductivity Testing Under Simulated Reservoir Conditions: Impact of Crushing, Embedment, and Diagenesis on Long-Term Production in Shales. *SPE J. SPE-191124-PA*. doi:https://dx.doi.org/10.2118/191124-PA

Montgomery, C., & Smith, M. (2010). Hydraulic Fracturing: History of an Enduring. *Journal of Petroleum Technology, 62*(12), 26-32. doi:10.2118/1210-0026

Muskat, M. (1946). *The Flow of Homogeneous Fluids through Porous Media.* New York: McGraw-Hill.

Nieto, C. (2007). *3D Characterization of Acidized Fracture Surfaces.* Thesis, Texas A&M University, Petroleum Engineering, College Station.

Odling, N. (1994). Natural Fracture Profiles, Fractal Dimensions, and Joint Roughness Coefficients. *Rock Mechanics and Rock Engineering*, 135-153.

Osniga, S., Zambrano-Narvez, G., & Chalaturnyk, R. (2015). Study of Geomechanical Properties of 3D Printed Sandstone Analogue. *ARMA 15-547*.

Shawn, M., & Jennings, J. (2014). Additive Manufacturing- Engineering Considerations for Moving Beyond 3D Printing. *International Ocean and Polar Engineering Conference* (pp. 307-313). Busan, Korea: ISOPE.

Stimpson, B. (1968). MOdeling Materials for Engineering Rock Mechanics. *Int.J. Rock Mech. Min. Sci, Vol 7*, 77-121.

Suarez-Rivera, R., Burghardt, J., Edelman, E., Stanchits, S., & Surdi, A. (2013). Considerations for Hydraulic Fracture Productivity. *ARMA-2013-666*.

Tatone, B., & Grasselli, G. (2010). A New 2D Discontinuity Roughness Parameter and its Correlation with JRC. *International Journal of Rock Mechanics and Mining Sceineces*, 1391-1400.

Tek, M., Coats, K., & Katz, D. (1962). The Effect of Turbulence on Flow of Natural Gas through Porous Reservoirs. *Journal of Petroleum Technology, 14*(07), 799-806. doi:10.2118/147-PA

Tse, R., & Cruden, D. (1979). Estimating Joint Roughness Coefficients. *International Journal of Rock Mechanics and Mining Sciences & Geomechanics*, 303-307.

Winner, R. (2018). *Experimental Evaluation of Novel Proppants for use in Hydraulic Fracturing of Unconventional reservoirs.* MS Thesis, Texas A&M University, College Station.

Woodman, J., Murphy, W., & Thomas, M. (2017). A Novel Approach to the Laboraotry Testing of Replica Discontinuities: 3D Printing Representative Morphologies. *ARMA.*

Yu, X., & Vayssade, B. (1991). Joint Profiles and Their Roughness Parameters. *International Journal of Rock Mechanics and Mining Sciences*, 333-336.

Zhang. (2014). *Creation and Impairment of Hydraulic Fracture Conductivity in Shale Formations.* Thesis, Texas A&M University, Petroleum Engineering, College Station, Texas.

Zhang, G., Karakus, M., Tang, H., Ge, Y., & Zhangg, L. (2014). A new method estimating the 2d joint roughness coefficient for discontinuity surfaces in rock masses. *International Journal of Rock Mechanics & Mining Sciences*, 191-198.